

AN ABSTRACT OF THE DISSERTATION OF

Xiaochun Duan for the degree of Doctor of Philosophy in

Electrical and Computer Engineering presented on June 8, 2005.

Title: Frequency Domain Steady-state Simulation of Oscillators

Abstract approved: \_\_\_\_\_

Kartikeya Mayaram

The focus of this work is on developing algorithms for frequency domain steady-state analysis of oscillators. Convergence problems associated with the frequency domain harmonic balance simulation of oscillators have been examined. Globally convergent homotopy methods have been combined with the harmonic balance method for robust high-Q oscillator simulation. Various homotopy options are evaluated leading to an algorithm that is applicable to a wide variety of oscillator circuits. Two new approaches have also been developed for the simulation of ring oscillators using the harmonic balance method. These include a single-delay cell method and a multiple-probe method. The new methods that have been proposed are robust compared to traditional methods and readily converge for a wide range of single-ended and differential oscillators. They enable harmonic balance simulation of “difficult-to-converge” oscillator circuits.

# Report Documentation Page

Form Approved  
OMB No. 0704-0188

Public reporting burden for the collection of information is estimated to average 1 hour per response, including the time for reviewing instructions, searching existing data sources, gathering and maintaining the data needed, and completing and reviewing the collection of information. Send comments regarding this burden estimate or any other aspect of this collection of information, including suggestions for reducing this burden, to Washington Headquarters Services, Directorate for Information Operations and Reports, 1215 Jefferson Davis Highway, Suite 1204, Arlington VA 22202-4302. Respondents should be aware that notwithstanding any other provision of law, no person shall be subject to a penalty for failing to comply with a collection of information if it does not display a currently valid OMB control number.

1. REPORT DATE <b>08 JUN 2005</b>		2. REPORT TYPE		3. DATES COVERED <b>00-00-2005 to 00-00-2005</b>	
4. TITLE AND SUBTITLE <b>Frequency Domain Steady-state Simulation of Oscillators</b>				5a. CONTRACT NUMBER	
				5b. GRANT NUMBER	
				5c. PROGRAM ELEMENT NUMBER	
6. AUTHOR(S)				5d. PROJECT NUMBER	
				5e. TASK NUMBER	
				5f. WORK UNIT NUMBER	
7. PERFORMING ORGANIZATION NAME(S) AND ADDRESS(ES) <b>Oregon State University, School of Electrical Engineering and Computer Science, 1148 Kelley Engineering Center, Corvallis, OR, 97331-5501</b>				8. PERFORMING ORGANIZATION REPORT NUMBER	
9. SPONSORING/MONITORING AGENCY NAME(S) AND ADDRESS(ES)				10. SPONSOR/MONITOR'S ACRONYM(S)	
				11. SPONSOR/MONITOR'S REPORT NUMBER(S)	
12. DISTRIBUTION/AVAILABILITY STATEMENT <b>Approved for public release; distribution unlimited</b>					
13. SUPPLEMENTARY NOTES					
14. ABSTRACT <b>The focus of this work is on developing algorithms for frequency domain steady-state analysis of oscillators. Convergence problems associated with the frequency domain harmonic balance simulation of oscillators have been examined. Globally convergent homotopy methods have been combined with the harmonic balance method for robust high-Q oscillator simulation. Various homotopy options are evaluated leading to an algorithm that is applicable to a wide variety of oscillator circuits. Two new approaches have also been developed for the simulation of ring oscillators using the harmonic balance method. These include a single-delay cell method and a multiple-probe method. The new methods that have been proposed are robust compared to traditional methods and readily converge for a wide range of single-ended and differential oscillators. They enable harmonic balance simulation of ?difficult-to-converge? oscillator circuits.</b>					
15. SUBJECT TERMS					
16. SECURITY CLASSIFICATION OF:			17. LIMITATION OF ABSTRACT	18. NUMBER OF PAGES	19a. NAME OF RESPONSIBLE PERSON
a. REPORT <b>unclassified</b>	b. ABSTRACT <b>unclassified</b>	c. THIS PAGE <b>unclassified</b>			

@ Copyright by Xiaochun Duan

June 8, 2005

All Rights Reserved

Frequency Domain Steady-state Simulation of Oscillators

by

Xiaochun Duan

A DISSERTATION

submitted to

Oregon State University

in partial fulfillment of  
the requirements for the  
degree of

Doctor of Philosophy

Presented June 8, 2005  
Commencement June 2006

Doctor of Philosophy dissertation of Xiaochun Duan presented on June 8, 2005.

APPROVED:

---

Major Professor, representing Electrical and Computer Engineering

---

Associate Director of the School of Electrical Engineering and Computer Science

---

Dean of the Graduate School

I understand that my dissertation will become part of the permanent collection of Oregon State University libraries. My signature below authorized release of my dissertation to any reader upon request.

---

Xiaochun Duan, Author

## ACKNOWLEDGEMENTS

First and foremost, I would like to thank my advisor Dr. Kartikeya Mayaram for his continuous support and skillful guidance throughout my Ph.D. studies. Without his trust and encouragement I would not have been able to finish this Ph.D. program. It's hard for me to find the most suitable word to express my appreciation. He was so patient in reviewing my drafts of papers and dissertation. He showed me the way to present my work. He is always there to listen to and give valuable advice for any problems I have. I feel so lucky to be able to study under his guidance and what I learned from him will definitely benefit my whole career.

I would like to thank Dr. Yun-Shik Lee, Dr. Terri Fiez, Dr. Huaping Liu, and Dr. Un-Ku Moon for being my committee members, and for their patience, time, and valuable suggestions during the various meetings for my Ph.D. program.

I would like to thank Dr. [Annette von Jouanne](#) for her understanding and support. Many thanks to all the members in the Energy Systems group where I spent the first year of my Ph.D. program.

My sincere thanks to all the members in the AMS group for their help and friendship. Special thanks to Yutao Hu and Chengang Xu for their knowledge, help, and valuable discussions.

I would like to acknowledge the financial support from NSF, SRC and DARPA for this research.

Finally, I would like to thank my family, my parents, my sisters and my boyfriend, for their unconditional love, support and trust throughout these years.

## TABLE OF CONTENTS

1. INTRODUCTION .....	1
1.1 Motivation and Contribution .....	1
1.2 Dissertation Outline .....	3
2. FREQUENCY-DOMAIN HARMONIC BALANCE METHOD.....	6
2.1 Introduction .....	6
2.2 Harmonic Balance Equation Formulation.....	8
2.2.1 The Discrete Fourier Transform (DFT).....	8
2.2.2 Formulating Harmonic Balance Equations.....	9
2.3 Newton's Method for the Harmonic Balance Problem.....	11
2.4 Matrix-implicit Krylov-subspace Methods .....	14
2.5 Spectral Accuracy of the Harmonic Balance Method .....	15
2.6 Error Mechanisms.....	17
2.7 Summary .....	18
3. SIMULATION OF OSCILLATORS WITH THE HARMONIC BALANCE METHOD .....	19
3.1 Introduction .....	19
3.2 Oscillators .....	20
3.2.1 Oscillator Structures.....	20
3.2.2 Oscillator Analysis .....	24
3.3 Application of the Harmonic Balance Method for Oscillator Simulation.....	25
3.4 The Probe Technique .....	26

## TABLE OF CONTENTS (Continued)

	<u>Page</u>
3.4.1 The Two-level Method.....	29
3.4.2 Convergence Conditions and Challenges.....	30
3.5 Summary.....	32
4. FREQUENCY-DOMAIN SIMULATION OF HIGH-Q OSCILLATORS.....	33
4.1 Introduction.....	33
4.2 Convergence Problems in High-Q Oscillators.....	34
4.3 Theory of Homotopy Methods.....	35
4.3.1 Homotopy methods for DC operating point problem.....	37
4.3.2 Homotopy methods for time-domain steady-state analysis of oscillators.....	39
4.4 Homotopy Method Solver: HOMPACT.....	41
4.5 Homotopy Formulations for Frequency-Domain Simulation of Oscillators.....	43
4.6 Summary.....	50
5. FREQUENCY-DOMAIN SIMULATION OF HIGHLY NONLINEAR RING OSCILLATORS.....	51
5.1 Introduction.....	51
5.2 Convergence of Harmonic Balance Methods for Ring Oscillators.....	52
5.3 Ring Oscillator Phase Relationships.....	56
5.4 Single-delay Cell Method.....	59
5.4.1 Single-delay Cell Equivalent Circuit.....	59

## TABLE OF CONTENTS (Continued)

	<u>Page</u>
5.4.2 Matrix Formulation for Harmonic Balance Method.....	60
5.4.3 Modified Voltage Probe Method .....	62
5.4.4 Solution by Newton’s Method.....	62
5.4.5 Differential Ring Oscillator Simulation .....	64
5.4.6 Limitation .....	66
5.5 Multiple-probe Method.....	66
5.5.1 Application of Multiple Probes.....	66
5.5.2 Initial Guesses for Multiple Probes.....	69
5.5.3 Solution by Newton’s Method.....	69
5.5.4 Computational Effort Analysis .....	71
5.6 Summary .....	72
6. FREQUENCY DOMAIN SIMULATION OF RELAXATION OSCILLATORS .....	73
6.1 Relaxation Oscillator Frequency Spectrum .....	73
6.2 Aliasing Error for Relaxation Oscillator Simulation .....	74
7. EXAMPLES AND RESULTS.....	77
7.1 Frequency-Domain Simulation of High-Q Oscillators.....	77
7.1.1 High-Q Oscillator Examples.....	77
7.1.2 Moderate-Q Oscillator Examples .....	83
7.2 Frequency-Domain Simulation of Highly Nonlinear Ring Oscillators .....	84
7.2.1 Convergence Performance and Accuracy .....	85

## TABLE OF CONTENTS (Continued)

	<u>Page</u>
7.2.2 Computational Performance of the Single-delay Cell Method..	88
7.2.3 Computational Performance of the Multiple-probe Method .....	94
7.2.4 Multiple-probe Method for Non-ideal Delay Cells.....	95
7.2.5 Simulation of Ring Oscillators with Numerical Models .....	96
7.3 Summary .....	99
8. CONCLUSIONS .....	100
8.1 Summary of Contributions .....	100
8.2 Future Work .....	101
BIBLIOGRAPHY .....	103

## LIST OF FIGURES

<u>Figure</u>	<u>Page</u>
3.1	Block diagram of an LC oscillator. ....21
3.2	Block diagram of a ring oscillator. ....22
3.3	(a) Pole location for relaxation oscillators. (b) Exponential growth of circuit waveform for a relaxation oscillator. ....23
3.4	Negative resistance approach for oscillator analysis. ....24
3.5	Positive feedback approach for oscillator analysis. ....25
3.6	(a) Voltage probe. (b) Current probe. ....27
3.7	Oscillator simulation with the aid of the voltage probe. ....28
3.8	Probe current tracking curves for selecting an initial probe voltage. Use of the frequency from a pole-zero analysis provides a good initial guess for the probe voltage (minimum in the tracking curve). ....31
4.1	Probe current tracking curves. $f_o$ is actual oscillation frequency, $f_{pz}$ is the frequency from the pole-zero analysis, and $f$ is a guess for the oscillation frequency. ....35
4.2	Circuit schematic of the Pierce oscillator. $R_1=100K\Omega$ , $R_2=2.2K\Omega$ , $C_1=100pF$ , $C_2=100pF$ , $C_p=25pF$ , $C_c=99.5fF$ , $R_c=6.4\Omega$ , $L_c=2.55mH$ , $V_{cc}=12V$ , $\beta=100$ for the BJT. ....45
4.3	Solution traces for the Pierce oscillator with the initial probe amplitude equal to the DC solution. (a) Probe voltage as a function of $\lambda$ . (b) Oscillation frequency as a function of $\lambda$ . ....45
4.4	Solution traces for the Pierce oscillator with the initial probe amplitude equal to 1mV. (a) Probe voltage as a function of $\lambda$ . (b) Oscillation frequency as a function of $\lambda$ . ....46
4.5	Algorithm 1: A two-parameter embedding homotopy algorithm. ....47

## LIST OF FIGURES (Continued)

<u>Figure</u>	<u>Page</u>
4.6	The solution tracking process in a high-Q resonator. (a) The voltage in the outer loop and frequency in the inner loop. (b) The frequency in the outer loop and voltage in the inner loop.....48
4.7	Algorithm 2: Modified embedding algorithm for high-Q oscillator simulation.....50
5.1	Ring oscillator delay cells. (a) Basic delay cell. (b) Current starved delay cell . (c) Vanilla delay cell. (d) Cross-coupled load delay cell [39].....54
5.2	Circuit waveform during the Newton iterative process. (a) Use of a small damping factor. (b) Adaptive damping with voltage/current thresholds. ....55
5.3	Five-stage ring oscillator waveform. ....57
5.4	Phase relationship for a three-stage ring oscillator.....58
5.5	Single-delay cell equivalent circuit for ring oscillator simulation. ....60
5.6	Single-delay cell equivalent circuit with a voltage probe at $f = f_{osc}$ .....62
5.7	Single-delay cell equivalent circuit for a differential ring oscillator at $f \neq f_{osc}$ .....65
5.8	Single-delay cell equivalent circuit with a voltage probe for the differential ring oscillator at $f=f_{osc}$ . ....65
5.9	Newton iterative process for the fundamental and 2 <sup>nd</sup> harmonic at different nodes and different iterations. (a) initial guess, (b) iteration #1, (c) iteration #2. ....67
5.10	Ring oscillator simulation using multiple voltage probes.....68
6.1	Schematic of a CMOS relaxation oscillator.....73
6.2	Time-domain waveform and frequency spectrum for a relaxation oscillator.....74

## LIST OF FIGURES (Continued)

<u>Figure</u>	<u>Page</u>
6.3	Oscillation frequency solution from the harmonic balance method using a different number of harmonics.....75
6.4	Frequency spectrum from transient analysis and harmonic balance method with 128 harmonics. ....75
6.5	Time-domain waveform from the harmonic balance method with 128 harmonics. ....76
7.1	Solution traces for the Pierce oscillator using the new algorithm. (a) Probe voltage as a function of $\lambda$ . (b) Oscillation frequency as a function of $\lambda$ . ....78
7.2	Results from transient and homotopy based harmonic balance simulations of the Pierce oscillator.....80
7.3	Circuit schematic of the Pierce oscillator with MOS inverter. R1=1M $\Omega$ , R2=2.7K $\Omega$ , C1=55pF, C2=60pF, Cp=25pF, Cc=10fF, Rc=60 $\Omega$ , Lc=2H. ....81
7.4	Solution traces for the high Q Pierce oscillator (Pierce2) using the new algorithm. (a) Probe voltage as a function of $\lambda_1$ . (b) Oscillation frequency as a function of $\lambda_1$ .....82
7.5	Solution traces for the Pierce oscillator (Pierce1) with numerical models using the new algorithm. (a) Probe voltage as a function of $\lambda_1$ . (b) Oscillation frequency as a function of $\lambda_1$ . ....83
7.6	Circuit waveform during the Newton iterative process. (a) Single-delay cell method. (b) Multiple-probe method.....87
7.7	Results from transient, single-delay cell harmonic balance, and multiple-probe harmonic balance simulation of a 9-stage ring oscillator.....88
7.8	4-stage differential ring oscillator. ....91
7.9	Ring oscillator delay cells. (a) Maneatis load delay cell. (b) Lee/Kim delay cell. (c) Current-controlled delay cell.....92

## LIST OF FIGURES (Continued)

<u>Figure</u>		<u>Page</u>
7.10	Simulation results for the 4-stage differential ring oscillator (current-controlled delay cell). .....	93
7.11	9-stage stepped-buffer connected as a ring oscillator. Each stage is sized a factor of $e$ larger than the previous stage. ....	96
7.12	Ring oscillator simulation with substrate noise. $f_{osc}=0.414\text{GHz}$ , $f_{sub}=0.8\text{GHz}$ , $V_{sub}=10\text{mV}$ . ....	98
7.13	Simulation results for a 3-stage ring oscillator with substrate noise. ....	98

## LIST OF TABLES

<u>Table</u>	<u>Page</u>
5.1	Convergence performance comparison of different harmonic balance methods for ring oscillator simulation. × denotes no convergence in 300 iterations..... 52
5.2	Convergence properties of different ring oscillator circuits. × denotes no convergence under exact initial guess for oscillation frequency and probe voltage..... 53
7.1	Newton iteration information for each $\lambda_1$ step for the Pierce oscillator using Algorithm 1 and Algorithm 2. $\Delta\lambda_1$ is the $\lambda_1$ increment from the previous $\lambda_1$ point. .... 79
7.2	Results for various high-Q oscillators. .... 81
7.3	Comparison of the two-level method and homotopy method for moderate-Q oscillator circuits. # indicates circuits with numerical models, and × denotes circuits that fail to converge. .... 84
7.4	Convergence sensitivity to initial guess for different ring oscillator circuits using the new single-delay cell and multiple-probe methods..... 86
7.5	Comparison of the conventional approach with the new single-delay cell approach for ring oscillators..... 89
7.6	Comparison of simulation results for single-ended ring oscillators with different number of stages..... 90
7.7	Comparison of simulation results for differential ring oscillators with different number of stages. × denotes no convergence under exact initial guess for the oscillation frequency and probe voltage. .... 91
7.8	Simulation performance comparison for the four-stage differential ring oscillators with different delay cells using the single-delay cell approach..... 93
7.9	Comparison of the multiple-probe method with the single-probe method for ring oscillator simulation. .... 94

LIST OF TABLES (Continued)

<u>Table</u>		<u>Page</u>
7.10	Comparison of ring oscillator simulation with identical delay cells and mismatched cells using the multiple-probe method. ....	95
7.11	Ring oscillator simulation results with 2D numerical MOSFET models.....	97

# 1. INTRODUCTION

## 1.1 Motivation and Contribution

Oscillators are widely used in RF circuits to generate reference signals [1]. Phase noise, one of the prime characteristics in the design of RF and microwave communication systems can be determined only if the oscillator circuit operates in its periodic steady state. Therefore, periodic steady-state simulations of oscillators are extremely important. A periodic steady-state analysis can be performed using the frequency-domain harmonic balance method or the time-domain finite-difference or shooting method [2-4].

The harmonic balance method is a nonlinear large-signal frequency-domain technique that can be used for fast and accurate steady-state analysis [2-4]. It can achieve a superior accuracy compared to time-domain methods due to its exponential convergence behavior [5]. It is also well suited for RF system simulation where the spectral and dynamic range requirements necessitate accurate analysis of harmonic content with large frequency differences [6]. Noise in an oscillator is frequently measured and described in the frequency domain. Although the harmonic balance method is well suited for these applications, it is susceptible to convergence problems when applied to oscillator circuits [2, 3].

The standard technique for frequency-domain oscillator simulation using the harmonic balance method is to apply a voltage probe which converts the oscillator circuit into a set of closely related numerically more efficient forced circuits [7]. The voltage probe is usually implemented with a two-level Newton method. The success of the two-level method, however, depends on 1) a close initial guess for the oscillation frequency and the probe voltage, and 2) the convergence of the bottom-level probe-forced circuit equations. Depending on the type of oscillator

the two-level Newton method fails to converge because a good initial guess can not be provided (high-Q oscillators) [8, 9] or the bottom-level equations fail to converge (highly-nonlinear oscillators, e.g., ring oscillators). For this reason, alternate approaches have to be studied. In this work, new algorithms and techniques have been developed for the efficient and robust simulation of both high-Q LC oscillators and highly nonlinear ring oscillators.

A detailed analysis in [8, 9] shows that a continuation method in conjunction with the voltage probe of [7] can be successfully used to simulate a high-Q oscillator. A multistage continuation approach for oscillator simulation using a Hopf bifurcation is also proposed in [10]. However, the specific details of the continuation methods are not provided [8–10]. This thesis explores the use of homotopy methods [11, 12] for the steady-state simulation of high-Q oscillators in the frequency domain.

Homotopy methods are globally convergent numerical techniques for solving nonlinear algebraic equations. They have been used extensively for finding the dc operating points of “difficult-to-solve” nonlinear circuits [12-15]. Recently, homotopy methods have also been applied to the steady-state analysis of oscillators in the time domain [16-18]. However, the use of homotopy methods with frequency-domain methods has not been previously studied. This work examines artificial parameter homotopy methods for oscillator steady-state simulation with the harmonic balance method [19]. Different embedding techniques are compared and evaluated. A robust and efficient embedding is identified and demonstrated to work well for a wide variety of LC oscillator circuits.

Previous work using the harmonic balance method for oscillator simulation has focused on LC oscillators which have near sinusoidal waveforms [7-9]. Some of these techniques can be applied to simulate ring oscillators, but due to the

highly nonlinear nature of the circuit, convergence problems exist [20]. Commercial harmonic balance tools use results from a time-domain transient analysis for simulating ring oscillators. The initial guesses thus achieved are nearly the same as the solution from the frequency-domain harmonic balance method and the convergence problem in the frequency-domain simulation of ring oscillators is not actually addressed. More importantly this approach cannot be extended to the simulation of voltage controlled ring oscillators in a RF system where transient analysis is no longer efficient due to the presence of mixer circuits.

In this work, convergence problems associated with the frequency-domain simulation of highly nonlinear ring oscillators have been examined. Two efficient and robust methods, a single-delay cell method [21, 22] and a multiple-probe method, are proposed for robust frequency-domain ring oscillator simulation using the harmonic balance method. Both approaches exploit the periodic structure of a ring oscillator and have been tested on a variety of single-ended and differential ring oscillators. They converge robustly for circuits where the conventional methods fail.

The application of the harmonic balance method to relaxation oscillator simulation is also investigated. It is shown that due to accuracy as well as convergence problems, the standard harmonic balance method is not suitable for relaxation type oscillators which have sharp waveform transitions.

## **1.2 Dissertation Outline**

This dissertation is organized as follows. Chapter 1 provides the motivation and contributions of this work. In Chapter 2, the frequency-domain harmonic balance method is reviewed. The equation formulation, solution strategy, spectral accuracy and the error mechanisms for the harmonic balance method are

introduced. Oscillator simulation using the harmonic balance method is presented in Chapter 3. First, oscillator structures and analysis are introduced. Then the application of the harmonic balance method to simulation of oscillators is discussed. The concept of the probe is introduced and its implementation by the two-level method is presented. Convergence problems and challenges are then described.

Frequency-domain simulation of high-Q oscillators is presented in Chapter 4. The challenges in simulating high-Q oscillators are first discussed and the theory of homotopy methods is reviewed. This is followed with an algorithm in which the homotopy method is applied to robust frequency-domain high-Q oscillator simulation.

In Chapter 5 the frequency-domain simulation of highly nonlinear ring oscillators is discussed. The problems associated with ring oscillator simulation are first introduced. To overcome the convergence problems in ring oscillator simulation two new methods, a single-delay cell method and a multiple-probe method are proposed. In the single-delay cell method, an equivalent circuit with only one delay cell is used for ring oscillator simulation. A modified voltage probe technique is used for convergence. Implementation details are given, along with the limitations of this method. In the multiple-probe method, multiple probes are included into the ring oscillator circuit. A discussion on initial guesses and computational effort is provided.

The application of the harmonic balance method to simulation of relaxation oscillators is briefly investigated in Chapter 6.

Chapter 7 presents the simulation results for the new methods proposed in this work. These include simulations of high-Q oscillators with the new homotopy-based algorithm and simulation of ring oscillators using the single-

delay cell and multiple-probe methods. Conclusions and future work are summarized in Chapter 8.

## 2. FREQUENCY-DOMAIN HARMONIC BALANCE METHOD

### 2.1 Introduction

With the rapid growth of the radio frequency (RF) integrated circuit market, there is an increasing demand to accurately simulate system performance before fabrication [2-4]. Many system characteristics, such as distortion, power, frequency, and noise, can be properly determined only if the circuit operates in its periodic steady-state domain. For this reason, periodic steady-state simulations of RF circuits are extremely important.

A trivial method for determining the steady-state response is to run a transient analysis and wait for all the waveforms to settle to their periodic steady state. However, this may be inefficient and, in some cases, not suitable for simulating RF systems with high-Q filters and wide frequency separations. In these cases, a long transient needs to be simulated to make sure the effects of the initial conditions die out and the time-step used by the numerical integration algorithm needs to be chosen small enough to capture the highest frequency of interest. Therefore, a large number of time points have to be simulated. To overcome the difficulty with the conventional transient simulation, steady-state solution is computed directly in the time domain by the finite-difference method or the shooting method, and in the frequency domain by the harmonic balance method [2-4].

The finite-difference method is not as widely used as the shooting method since it requires a large amount of memory and tends to have more convergence problems than the shooting method [2]. The shooting method is a popular time-domain method in which a two-point boundary value problem is formulated. It uses the transient analysis over one period to obtain the final value at the end of

the period, so it can be viewed as an accelerated transient method. The acceleration is obtained by adjusting the initial condition at the beginning of each one-period transient simulation. The shooting method works well for highly nonlinear circuits since it is based on a time-domain analysis and has the ability to handle the nonlinear behavior of circuits. However, the shooting method is not suitable for circuits with wide frequency separations and it cannot handle distributed devices commonly encountered in RF simulation [2].

The harmonic balance (HB) method is a frequency-domain algorithm used for high accuracy computation of the periodic steady state of RF circuits [2-3]. It is well suited for RF system simulation where the spectral and dynamic range requirements necessitate accurate analysis of harmonic content with large frequency differences [6]. Because it is a frequency-domain technique, distributed models can be easily and accurately included in the simulation [2]. With a Krylov subspace solver, the harmonic balance method can be applied to full-chip simulation with multi-tone excitations [6].

This chapter is organized as follows. The harmonic balance method formulation is reviewed in Section 2.2. The discrete Fourier transform for a periodic signal is also presented. Newton's method for the harmonic balance problem is described in Section 2.3. The matrix implicit Krylov subspace method is briefly discussed in Section 2.4. The spectral accuracy of the harmonic balance method compared to the time-domain methods is described in Section 2.5. The error mechanisms in the harmonic balance method are introduced in Section 2.6, and a chapter summary is provided in Section 2.7.

## 2.2 Harmonic Balance Equation Formulation

The harmonic balance method is a frequency-domain method where the circuit waveforms are represented by the Fourier sine and cosine series [2-3]. This approximation of a time-domain waveform as a Fourier series naturally and efficiently guarantees that the solution obtained is indeed the periodic steady state of the system. The unknowns in the harmonic balance method are the frequency-domain Fourier coefficients and not the time-domain waveforms, whereby the dynamic aspects of the problem are eliminated.

### 2.2.1 The Discrete Fourier Transform (DFT)

The harmonic balance method formulates circuit equations in the frequency domain. The Fourier transform is used to transform the circuit unknowns between the time and frequency domains. Since the time-domain circuit unknowns are real-valued waveforms, a simplified version of the standard discrete Fourier transform (DFT) is introduced here.

A periodic waveform with period  $T$  can be represented by a Fourier series:

$$x(t) = X_0 + \sum_{i=1}^{\infty} X_i^c \cos(\omega_i t) + X_i^s \sin(\omega_i t) \quad (2.1)$$

where  $\omega_i$  is the frequency for the  $i$ th harmonic,  $X_0$  is the DC value and  $X_i^c$  ( $X_i^s$ ) is the Fourier coefficient of the cosine (sine) part of the  $i$ th harmonic. To make the problem computationally tractable, it is necessary to truncate the frequencies to a finite set. If the energy in harmonics higher than  $K$  is negligible, the waveform  $x(t)$  can be approximated as

$$x(t) \approx X_0 + \sum_{i=1}^K X_i^c \cos(\omega_i t) + X_i^s \sin(\omega_i t) \quad (2.2)$$

As the spectrum of  $x(t)$  is finite, it is possible to sample the time-domain waveform at a finite number of time points and calculate the Fourier coefficients. To get  $2K+1$  Fourier coefficients, at least the same number of sampled time points have to be used. This results in a set of  $2K+1$  equations with  $2K+1$  unknowns:

$$\begin{bmatrix} x_0 \\ x_1 \\ x_2 \\ \vdots \\ x_{2K-1} \\ x_{2K} \end{bmatrix} = \Gamma^{-1} \begin{bmatrix} X_0 \\ X_1^c \\ X_1^s \\ \vdots \\ X_K^c \\ X_K^s \end{bmatrix} \quad (2.3)$$

where

$$\Gamma^{-1} = \begin{bmatrix} 1 & \cos \omega_1 t_0 & \sin \omega_1 t_0 & \cdots & \cos \omega_K t_0 & \sin \omega_K t_0 \\ 1 & \cos \omega_1 t_1 & \sin \omega_1 t_1 & \cdots & \cos \omega_K t_1 & \sin \omega_K t_1 \\ 1 & \cos \omega_1 t_2 & \sin \omega_1 t_2 & \cdots & \cos \omega_K t_2 & \sin \omega_K t_2 \\ \vdots & \vdots & \vdots & & \vdots & \vdots \\ 1 & \cos \omega_1 t_{2K} & \sin \omega_1 t_{2K} & \cdots & \cos \omega_K t_{2K} & \sin \omega_K t_{2K} \end{bmatrix} \quad (2.4)$$

is the inverse DFT, and  $x_k$  is the value of  $x(t)$  sampled at equally spaced time points  $t_k$  ( $k = 0, 1, \dots, 2K$ ), where  $t_k = kT/(2K+1)$ . This system is invertible and can be compactly written as  $\Gamma^{-1}X = x$ . Inverting  $\Gamma^{-1}$  gives  $\Gamma x = X$ .  $\Gamma$  (DFT) and  $\Gamma^{-1}$  (inverse DFT) are a discrete Fourier transform pair.

### 2.2.2 Formulating Harmonic Balance Equations

The circuit behavior can be described in the time domain by a system of equations:

$$i(x(t)) + \frac{d}{dt}q(x(t)) + s(t) = 0 \quad (2.5)$$

where  $x$  is the vector of circuit waveforms (voltage/current),  $i$  is a function of the contributions from the nonreactive elements to the circuit equations,  $q$  (charge/flux) is the contribution from reactive elements, and  $s$  is an input source.

Let the circuit be driven by a single periodic input source with period  $T$ . Then the circuit steady-state response  $x(t)$  will also be periodic and a truncated Fourier series can be used to approximate the signal as in Eq. (2.2). Using the Fourier coefficients as unknowns, the circuit equations can be formulated in the frequency domain as

$$\Gamma i(\Gamma^{-1}X) + \Omega \Gamma q(\Gamma^{-1}X) + S = 0 \quad (2.6)$$

where  $X$  is the vector of circuit waveforms in the frequency domain represented by their Fourier coefficients,  $\Gamma$  and  $\Gamma^{-1}$  are the discrete Fourier transform matrix pair,  $S$  is the frequency-domain representation of the stimulus vector,  $\Omega$  is a block-diagonal matrix representing the time derivative operation [2]:

$$\Omega = \begin{bmatrix} 0 & & & \\ & \omega_1 & & \\ & & \ddots & \\ & & & \omega_K \end{bmatrix} \quad \omega_k = \begin{bmatrix} 0 & \omega_k \\ -\omega_k & 0 \end{bmatrix} \quad (2.7)$$

where  $\omega_k$  is the frequency for the  $k$ th harmonic. Since each frequency requires two Fourier coefficients, except DC, the number of Fourier coefficients for each circuit waveform is  $2K+1$ . If there are  $N$  waveforms in the circuit, the total number of unknowns is  $N(2K+1)$  [23-24].

The harmonic balance equations can be seen as KCL formulated in the frequency domain where the frequency spectrum at each node is balanced. The

advantage of this set of equations is that the time domain derivative operation ( $\frac{d}{dt}$ ) is changed into an algebraic multiplication operation ( $\Omega$ ) in the frequency domain. This directly yields the solution in the steady state.

The harmonic balance method can also be written in the time domain by converting Eq. (2.6) from the frequency domain to time domain:

$$i(x) + \Gamma^{-1}\Omega\Gamma q(x) + s = 0 \quad (2.8)$$

where  $x$  and  $s$  are the vectors of  $2K+1$  time-domain samples of unknown waveforms and stimuli, respectively. From Eqs. (2.5) and (2.8) we can see that the time derivative in Eq (2.5) is approximated by  $D = \Gamma^{-1}\Omega\Gamma$  in the harmonic balance method. The time-domain differentiation matrix  $D$  is a block-dense, real matrix. The harmonic balance method can, therefore be viewed as a finite-difference method of order  $K$ , the order of the Fourier truncation [5].

### 2.3 Newton's Method for the Harmonic Balance Problem

The harmonic balance method results in a system of nonlinear algebraic equations. Newton's method is applied to solve these equations iteratively. This application results in the iteration

$$J^{(i)}(X^{i+1} - X^i) = -F(X^i) \quad (2.9)$$

where  $i$  is the Newton iteration index.  $J^{(i)}$  is the  $i$ th Newton iteration Jacobian

$$J^{(i)} = \Gamma G^{(i)} \Gamma^{-1} + \Omega \Gamma C^{(i)} \Gamma^{-1} \quad (2.10)$$

where  $G$  and  $C$  are block diagonal matrices, with the diagonal elements representing the circuit linearized at the sampled time points:

$$G = \begin{bmatrix} \bar{G}_0 & & & \\ & \bar{G}_1 & & \\ & & \ddots & \\ & & & \bar{G}_{2K} \end{bmatrix} \quad (2.11)$$

$$C = \begin{bmatrix} \bar{C}_0 & & & \\ & \bar{C}_1 & & \\ & & \ddots & \\ & & & \bar{C}_{2K} \end{bmatrix} \quad (2.12)$$

where  $\bar{G}_k = \left. \frac{\partial i(x)}{\partial x} \right|_{x_k}$  and  $\bar{C}_k = \left. \frac{\partial q(x)}{\partial x} \right|_{x_k}$  are the  $N \times N$  linearized conductance and capacitance matrices at time point  $t_k$ , respectively. These linearized matrices can be obtained by multiple small-signal analyses around the operating points specified at each sample time point.

For an arbitrary nonlinearity, the Fourier coefficients of the response can not be computed directly from the Fourier coefficients of the stimulus. This is possible only for some special cases [25]. Therefore, the nonlinear device is first evaluated in the time domain and then transformed to the frequency domain by the Fourier transform.

Let's consider a nonlinear resistive example

$$i = i(v) \quad (2.13)$$

where  $i$  is the current through the nonlinear resistor and  $v$  is the voltage across it. The frequency domain equation for the nonlinear resistor is given by

$$I = \Gamma i(\Gamma^{-1}V) \quad (2.14)$$

where  $I$  and  $V$  are the Fourier coefficients of the current and voltage, respectively. The frequency-domain voltage Fourier coefficients are first transformed into a

time-domain circuit waveform  $v = \Gamma^{-1}V$  and then the current  $i(v)$  is evaluated in the time domain. The frequency-domain current Fourier coefficients are obtained by the use of the Fourier transform  $\Gamma$  on the time-domain current waveform,  $i$ .

When using Newton's method, the frequency-domain current is linearized at each iteration

$$\begin{aligned} I^{(i+1)} &= \Gamma i(\Gamma^{-1}V^{(i+1)}) = \Gamma i(\Gamma^{-1}V^{(i)}) + \Gamma \frac{\partial i(\Gamma^{-1}V^{(i)})}{\partial(\Gamma^{-1}V^{(i)})} \frac{\partial(\Gamma^{-1}V^{(i)})}{\partial V^{(i)}} (V^{(i+1)} - V^{(i)}) \\ &= \Gamma(G(v^{(i)})v^{(i+1)} + (i(v^{(i)}) - G(v^{(i)})v^{(i)})) \end{aligned} \quad (2.15)$$

From Eq. (2.15) we can see that to evaluate the nonlinear elements in the frequency domain via the time domain, a time-domain companion network [26] can be used. The only difference is that the companion network needs to be transformed to the frequency domain by the Fourier transform matrix  $\Gamma$ .

For linear circuits, the  $G$  and  $C$  matrices are independent of the voltages which results in an iteration-invariant block-diagonal Jacobian matrix. Newton's method converges in one iteration, and the harmonic balance method is equivalent to a phasor analysis. For nonlinear circuits, the Jacobian is no longer block diagonal. The off-diagonal elements represent the frequency coupling whose strength depends on the nonlinearity of the circuit [2].

Newton's method may only converge if the initial guess is close enough to the solution. Thus, a good initial guess is important in determining the likelihood of convergence. For many circuits, the DC operating point can be used as a good initial guess. An initial guess can also be generated by linearizing the circuit at the DC operating point, applying the stimulus, and performing a phasor analysis at each frequency.

One feature of Newton's method is that, once a solution has been found, the resulting harmonic Jacobian represents a linearization of the circuit about its time

varying operating point. This can be used in small-signal time varying analysis such as mixer noise analysis or phase noise calculation for oscillators.

## 2.4 Matrix-implicit Krylov-subspace Methods

The Jacobian matrix of the harmonic balance method is a dense matrix of size  $N(2K+1)$ . The factorization of such a large dense matrix by a direct method is prohibitively expensive, which limits the application of the harmonic balance method to larger circuits.

Krylov subspace methods have been shown to be effective when applied to the solution of a large-scale system of harmonic balance equations. The Krylov subspace methods involve only matrix vector products. Therefore these methods can be easily applied in situations where the matrix may not be directly available, and generating, storing, and multiplying with that matrix involves significant overhead. For instance, in the harmonic balance method, the coefficient matrix is available as a sequence of transforms which can be efficiently applied to a vector [27-31].

The convergence rate of a Krylov subspace method strongly depends on the condition number or spectral properties of the coefficient matrix. The idea of preconditioning is to transform the original linear system into one that is equivalent with the same solution, but has more favorable spectral properties or condition number. The preconditioner is a matrix that performs this transformation. One way to design a preconditioner is to construct a matrix that approximates the coefficient matrix, and is easy to invert. The successful use of Krylov subspace methods in most situations, is determined by the ability to form an appropriate preconditioner [27-31].

In the frequency-domain formulation of the harmonic balance method, the most commonly used preconditioner is a block diagonal matrix which is formed from the Jacobian matrix by only keeping the linear part. This preconditioner can be easily and efficiently formed and inverted due to its block-diagonal structure. The block-diagonal preconditioner has been shown to be very effective for a large number of weakly nonlinear problems. However, it becomes increasingly ineffective for strongly nonlinear problems because it becomes a poor approximation of the harmonic Jacobian matrix [27].

Adaptive preconditioners [28-29] are formed by neglecting the small harmonics of nonlinear conductances and capacitances. This process corresponds to retaining, in addition to the block-diagonal entries, only the most essential non-diagonal entries of the Jacobian matrix.

Recently, the Jacobian matrix from a lower-order finite difference method on a uniform grid was also used as a preconditioner. This was possible since the time-domain formulation of the harmonic balance method is a finite-difference method in disguise [30-31]. The Jacobian matrix from a finite-difference method is a good approximation of the Jacobian matrix of the harmonic balance method formed in the time domain. The order of the time-domain integration method determines the bands of the blocks.

With more complex preconditioners, one can expect the computational effort to reduce due to a decrease in the number of linear iterations. However, there will be an increased effort in factoring the preconditioners.

## **2.5 Spectral Accuracy of the Harmonic Balance Method**

Time-domain methods (finite-difference method and shooting method) compute the steady state by first discretizing the solution domain  $[0, T]$ . The time

derivatives are approximated with finite-order integration formulas. For example, for the  $K$ -th-order BDF formula, the time derivative of a function is computed using values of the function at  $K$  nearby time points [2]. For this reason, the approximation of the derivative in the time domain captures only the local behavior of the function. These time-domain methods are exact for polynomials of order  $\leq K$ . In other words, the solution is represented by a sequence of low-order polynomials connected at the discrete time-points. These methods can, therefore, at best achieve polynomial convergence with global errors, i.e.,  $O(h^K)$  [5].

The frequency-domain harmonic balance method approximates the solution waveforms using a weighed Fourier basis. The time-derivative of this approximation can be computed exactly as

$$\dot{x}(t) = \sum_{i=1}^K (\omega_i X_i^s \cos(\omega_i t) - \omega_i X_i^c \sin(\omega_i t)) \quad (2.16)$$

If the circuit waveform is sampled at  $2K+1$  uniformly distributed time points, then the time derivative at each time point is approximated with

$$\begin{bmatrix} \dot{x}_0 \\ \dot{x}_1 \\ \dot{x}_2 \\ \vdots \\ \dot{x}_{2K-1} \\ \dot{x}_{2K} \end{bmatrix} = \Gamma^{-1} \Omega \Gamma \begin{bmatrix} x_0 \\ x_1 \\ x_2 \\ \vdots \\ x_{2K-1} \\ x_{2K} \end{bmatrix} \quad (2.17)$$

Since  $\Gamma^{-1} \Omega \Gamma$  is a dense matrix, the time derivative of the circuit waveform at each time point is computed using values of the circuit waveforms at  $2K+1$  time points. Since these time points span the whole period of the circuit waveform, the time derivative in the harmonic balance method includes the global behavior of a function.

Due to the global nature of the harmonic balance method, as  $i \rightarrow \infty$  the  $i$ th Fourier coefficient  $X_i$  decays rapidly if the solution waveform is smooth. This rapid decay of the coefficients means that the truncated Fourier approximation of a solution expanded using a few additional terms (by slightly increasing  $K$ ) represents an exceedingly good approximation of the solution, a property known as spectral accuracy, exponential convergence, or infinite-order accuracy. The harmonic balance method will not achieve spectral accuracy if a discontinuity is present in the solution waveforms or one of their derivatives. If the device models are  $p$ -times continuously differentiable functions and periodic in all its derivatives, then the errors for the harmonic balance method will be  $O(K^{-p})$  [5].

## 2.6 Error Mechanisms

The errors in the harmonic balance method come from the truncation of the frequency spectrum to some finite order and the use of a finite-order discrete Fourier transform. This error can be split into two parts, a truncation error and an aliasing error [2].

Consider a circuit with periodic or quasi-periodic solutions. Let  $F$  be the sum of currents at every node and every frequency.  $\Lambda_K$  is defined as the truncated set of frequencies. Let  $F_{exact}$  be the result when the circuit equations are evaluated without an error at all frequencies. Then the truncation error is defined as

$$F_{trunc}(V, k) = \begin{cases} 0 & \text{if } \omega_k \in \Lambda_K \\ F_{exact}(V, k) & \text{otherwise.} \end{cases} \quad (2.18)$$

Thus,  $F_{trunc}$  represents all currents generated by the circuit at frequencies other than those in  $\Lambda_K$  [2].

Aliasing errors are introduced when a time-domain waveform is converted into a frequency-domain spectrum using a finite-order discrete Fourier transform. Aliasing is caused by using too few time points to represent the time waveform. The Nyquist criterion states that to avoid aliasing errors, the sampling frequency should be at least twice the highest frequency present in the time-domain waveform [32]. If not, an error is introduced in the low-frequency Fourier coefficients. In this sense the harmonic balance method is more accurate for band-limited signals where the error from aliasing does not corrupt the frequency spectrum. The only way to eliminate aliasing errors is to increase the number of data points by oversampling the time-domain waveform.

The aliasing error is generally as large as or larger than the truncation error [2]. One approach to estimate the error due to the truncation and aliasing is to simply increase the number of frequencies used in the Fourier series representation of the circuit unknowns and re-simulate the circuit. However, this method of estimating the error is an inexpensive way of determining whether enough frequencies have been included in the harmonic balance analysis after a solution has been computed.

## **2.7 Summary**

This chapter first presented an overview of the harmonic balance algorithm. The harmonic balance method overcomes several difficulties faced by time-domain methods by solving the system of equations in the frequency domain. It also provides higher spectral accuracy compared to the time-domain methods. The formulation of the harmonic balance equations and solution with Newton's method is described. Error mechanisms in the harmonic balance method have also been discussed.

### 3. SIMULATION OF OSCILLATORS WITH THE HARMONIC BALANCE METHOD

#### 3.1 Introduction

Oscillators are widely used in many applications such as phase-locked loops (PLL) and frequency synthesizers to generate reference signals [1]. Phase noise is an important characteristic of oscillators and can be determined only if the circuit operates in its periodic steady state [33-34]. For this reason, periodic steady-state simulations of oscillators are extremely important [2-3].

The periodic steady-state analysis can be done in either the time domain or in the frequency domain. The frequency-domain harmonic balance analysis is spectrally more accurate than the time-domain method since low-order integration is typically used in the latter. It is also very efficient for RF system simulation since it can handle the wide spread of frequencies naturally.

The harmonic balance method has been applied to oscillator simulation by adding the unknown oscillation frequency to the set of circuit state variables. However, oscillator simulation using the harmonic balance method has proven to be difficult due to a small region of convergence and the existence of the degenerate DC solution [2]. Careful implementation and special techniques must be used for convergence [2, 7].

In this chapter, the basic oscillator structures and their operation are first introduced in Section 3.2. The application of the harmonic balance method to oscillator simulation is reviewed in Section 3.3. The probe technique for improving the convergence in frequency-domain oscillator simulation is described in Section 3.4.

## 3.2 Oscillators

Most electronic signal processing systems require frequency or time reference signals. In communication systems oscillators generate the signals to modulate the baseband message signal in transmitters, and process the received signals in receivers. There are many different kinds of oscillators for various applications.

### 3.2.1 Oscillator Structures

Oscillators can be broadly classified into three categories: harmonic oscillators, ring oscillators, and relaxation oscillators [1].

The most common harmonic oscillators are those that use resonant circuits consisting of inductors and capacitors. Harmonic oscillators that use LC resonant circuits are known as LC oscillators. A typical LC oscillator is made up of three distinct blocks as shown in Fig. 3.1. The amplifier supplies energy to maintain oscillations in the circuit. The LC tank circuit alternately stores energy in the inductor and the capacitor. A portion of the output of the LC network is fed back to the input of the amplifier through a positive feedback network. This helps to sustain oscillations by overcoming the effect of the damping caused by the internal and load resistances of LC tanks.

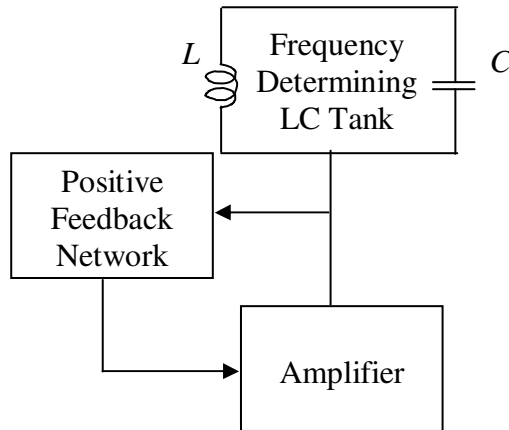


Figure 3.1: Block diagram of an LC oscillator.

The operating or center frequency ( $f$ ) of the LC oscillator is fixed by the resonant frequency of the LC tank circuit

$$f = \frac{1}{2\pi\sqrt{LC}} \quad (3.1)$$

An important quantity in the characterization of LC tank circuits is the quality factor,  $Q$ , which is defined as

$$Q = \omega \frac{\text{energy stored}}{\text{average power dissipated}} \quad (3.2)$$

The resonator  $Q$  strongly influences both the phase noise and power consumption of an oscillator. The inductor in an LC oscillator is usually the most critical circuit element in the design. Typically, the  $Q$  of the inductor dominates the total  $Q$  of the tank circuit.

Ring oscillators are resonator-less oscillators consisting of an odd number of single-ended inverters or an even/odd number of differential inverters with

appropriate connections. A single-ended ring oscillator structure is shown in Fig. 3.2. If each inverter is ideal this circuit is a form of negative feedback, but in reality each inverter exhibits a lagging phase shift arising from the propagation delay. Enough lagging phase shift (at least three inverters in the loop) added to the inversions ultimately turns the negative feedback into a positive feedback. As a result the circuit is unstable and oscillations occur [35]. In each half-period, the signal propagates around the loop with an inversion. Whereby the oscillation frequency for a ring oscillator is determined by

$$f = \frac{1}{2n\tau_d} \quad (3.3)$$

where  $n$  is the number of stages in the ring oscillator, and  $\tau_d$  is the time delay of one stage [35].

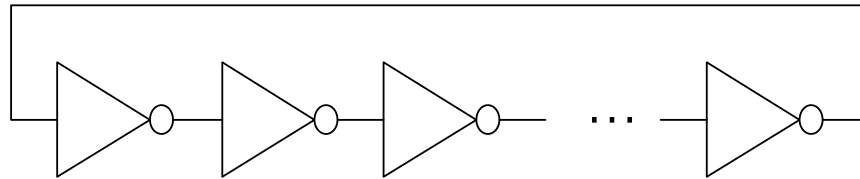


Figure 3.2: Block diagram of a ring oscillator.

The operation of a relaxation oscillator is very different from the other types of oscillators. Relaxation oscillators have poles located in the right half plane to make it an unstable circuit. Unlike LC oscillators, the poles for relaxation oscillators are real instead of complex as shown in Figure 3.3. Therefore, the signal amplitude will grow exponentially until some transistors are cut off [36].

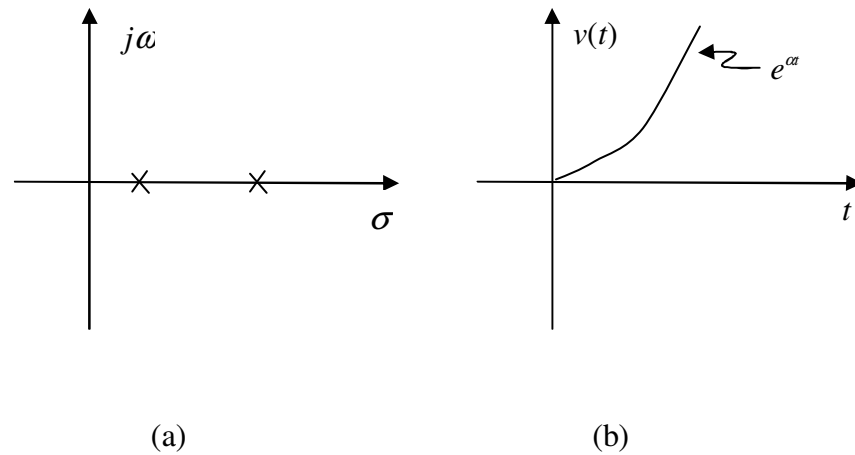


Figure 3.3: (a) Pole location for relaxation oscillators. (b) Exponential growth of circuit waveform for a relaxation oscillator.

The relaxation oscillator has two distinct phases of operation, a fast regenerative switching phase and a recovery phase. Oscillations in relaxation oscillators are commonly achieved by the charging and discharging of capacitors with a constant current between two threshold levels. The oscillation frequency of a relaxation oscillator is set by the charge/discharge rate of the capacitor and the difference between two separate threshold levels at the input of the regenerative element.

Oscillators employed in RF applications must meet stringent phase noise requirements, so LC type oscillators with a high quality factor are preferred. High-Q factors cannot be achieved in integrated implementations because of the availability of low Q inductors. The trend toward large-scale integration and low cost makes it desirable to implement oscillators on chip. Ring and relaxation oscillators have raised interest among circuit designers because they are very compact, simple and can operate at high speeds [1]. A ring oscillator can also readily yield output phases in quadrature.

### 3.2.2 Oscillator Analysis

To generate a periodic output, the oscillator circuit must have a self-sustaining mechanism that allows its own noise to grow and eventually become a periodic signal. There are two analysis points of view for oscillators, the negative resistance approach and the feedback approach [36].

The negative resistance concept is illustrated in Fig. 3.4. A *RLC* tank circuit has losses represented by the resistance  $R$ , so it cannot oscillate indefinitely as the stored energy is dissipated in the resistor for every cycle. To sustain oscillations the loss of energy must be compensated. An active network is used to generate a resistance equal to  $-R$ . In this case, the circuit can be seen as a lossless LC tank and the energy lost in  $R$  is replenished by the active circuit in every cycle.

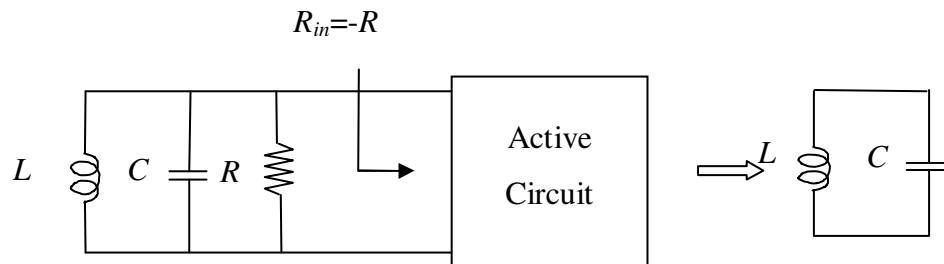


Figure 3.4: Negative resistance approach for oscillator analysis.

The feedback approach is illustrated in Fig. 3.5. The oscillator is viewed as a circuit with positive feedback where a portion of the output is combined in phase with the input. The closed-loop gain is given by

$$\frac{X_o}{X_s} = \frac{A(s)}{1 - A(s)B(s)} \quad (3.4)$$

where  $A(s)B(s)$  is the loop gain. The oscillation reaches its steady state when  $s$  is purely imaginary and

$$\begin{aligned} |A(j\omega_0)B(j\omega_0)| &= 1 \\ \angle A(j\omega_0) + \angle B(j\omega_0) &= 2\pi n \quad \text{where } n = 1, 2, 3, \dots \end{aligned} \quad (3.5)$$

where  $\omega_0$  is the oscillation frequency [1].

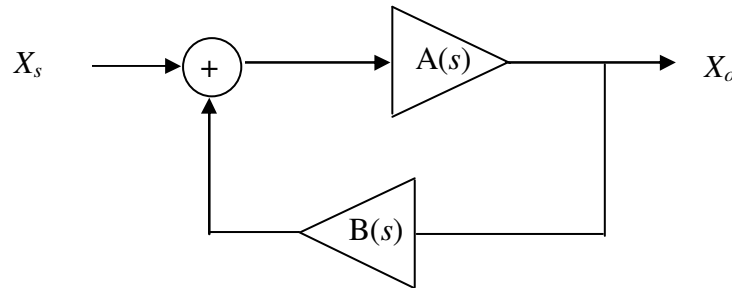


Figure 3.5: Positive feedback approach for oscillator analysis.

### 3.3 Application of the Harmonic Balance Method for Oscillator Simulation

An important application of the harmonic balance method is in determining the steady-state behavior of oscillators [2]. Oscillators present two problems not found in forced circuits. First, the period of oscillation is an unknown and must be determined. Second, there is no input to fix the phase. Thus, if one solution exists, then an infinite continuum of phase-shifted solutions exists. For these reasons, Eq. (2.6) is modified to handle oscillators by adding the fundamental frequency to the list of unknowns. An additional equation is also added to fix the phase. The common practice is to set the sine part of the fundamental of the chosen signal to zero [2].

$$\begin{aligned} F(X, \omega) &= \Gamma i(\Gamma^{-1} X) + \Omega(\omega) \Gamma q(\Gamma^{-1} X) + S = 0 \\ X_m^s(1) &= 0 \end{aligned} \quad (3.6)$$

This set of equations can be solved using Newton's method where the Jacobian is given by

$$J_{osc} = \begin{bmatrix} J & \frac{\partial F}{\partial \omega} \\ (e_m^s(1))^T & 0 \end{bmatrix} \quad (3.7)$$

with

$$\frac{\partial F}{\partial \omega} = \frac{\Omega \Gamma q(\Gamma^{-1} X)}{\omega} \quad (3.8)$$

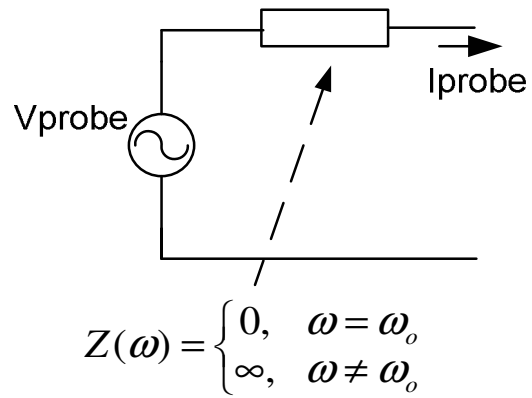
where  $J$  is the Jacobian in Eq. (2.10) and  $e_m^s(1)$  is the unit vector that selects the sine part of the first harmonic of the chosen signal.

This implementation is straightforward. However, without an extremely good initial guess for both the oscillation frequency and all the circuit unknowns, the method either tends to converge to the trivial DC solution, or fails to converge [7-9]. The reason for the convergence difficulty is that the unknown frequency is adjusted at every iteration along with the node voltages. The node voltages at the intermediate iterations do not satisfy KCL. Updating the frequency based on these node voltages can lead to divergence, or make convergence difficult.

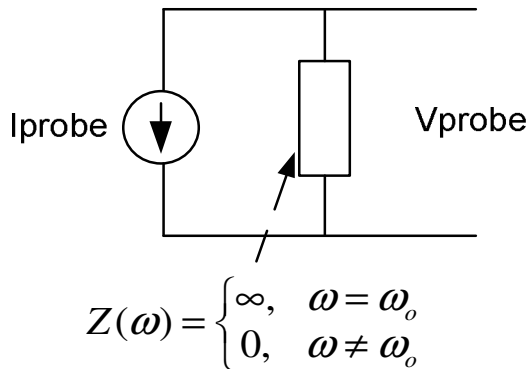
### 3.4 The Probe Technique

To handle the convergence problems encountered in frequency-domain oscillator simulation, Ngoya et al. [7] presented the idea of a probe which has become a standard technique for frequency-domain oscillator simulation. The probe can be a voltage probe or a current probe as shown in Fig. 3.6. A probe is composed of an ideal independent source (current source or voltage source for current or voltage probe, respectively) associated with a filter. The filter

electrically disconnects the probe from its termination for any frequency different from that of the probe source (a short circuit for the current probe, and an open circuit for the voltage probe).



(a)



(b)

Figure 3.6: (a) Voltage probe. (b) Current probe.

To simulate an oscillator the voltage probe is connected in parallel and the current probe is connected in series. The implementation of the current probe is not as straightforward as that of the voltage probe since the circuit must be broken at a certain point to insert the current probe. Furthermore, it's easier to specify an initial guess for a voltage than a current, so the voltage probe is more commonly used.

The simulation of an oscillator with the aid of the voltage probe is shown in Fig. 3.7 where the probe voltage and frequency keep changing until the solution is obtained when the probe current becomes zero. Then all the circuit equations are satisfied without the probe being a part of the circuit. In this case, the voltage probe is actually detached from the oscillator circuit. The advantage of the probe approach is that the simulation of an oscillator circuit is changed into a set of closely related forced circuits, which can be easily handled using the standard harmonic balance method.

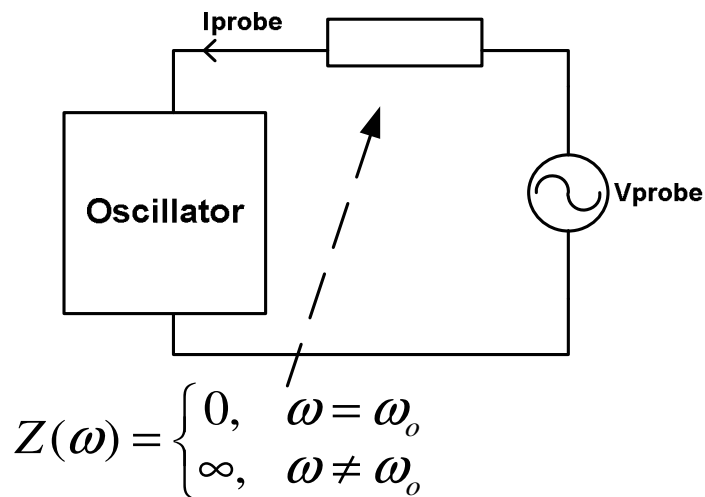


Figure 3.7: Oscillator simulation with the aid of the voltage probe.

The node at which the voltage probe is attached in the oscillator circuit influences the robustness of the approach. It is observed that better convergence is achieved if the voltage probe is attached at a high impedance node. The collector node of the BJT device or the drain node of the MOS device is usually a good choice.

### 3.4.1 The Two-level Method

The voltage probe is implemented by a two-level Newton method [7]. The bottom level of the two-level method solves the harmonic balance equations of the voltage-probe forced circuit. The voltage probe is implemented directly in the frequency domain with the corresponding branch constitutive equations. The sine part of the probe voltage is set to zero to fix the phase and thus selects one of the many equivalent solutions. The linear equations solved at each step of the bottom-level Newton method are given by

$$\begin{bmatrix} J & e_m^c(1) & e_m^s(1) \\ e_m^c(1)^T & 0 & 0 \\ e_m^s(1)^T & 0 & 0 \end{bmatrix} \begin{bmatrix} X^{(j+1)} \\ I_{probe}^{c(j+1)} \\ I_{probe}^{s(j+1)} \end{bmatrix} = \begin{bmatrix} RhsF^{(j)} \\ V_{probe} \\ 0 \end{bmatrix} \quad (3.9)$$

where  $J$  is the Jacobian in Eq. (2.10).  $e_m^c(1)$  ( $e_m^s(1)$ ) is the unit vector that selects the cosine (sine) part of the first harmonic of the chosen node to which the probe is attached.  $I_{probe}^c$  ( $I_{probe}^s$ ) is the cosine (sine) part of the probe current,  $RhsF$  is the right-hand-side vector of the circuit which includes the circuit stimulus and the contributions from nonlinear devices.

After getting the probe current from the bottom solution, the top-level solves the probe equations as shown in Eq. (3.10) to update the probe voltage and the frequency.

$$\begin{aligned}
I_{probe}^c(V_{probe}, \omega) &= 0 \\
I_{probe}^s(V_{probe}, \omega) &= 0
\end{aligned}
\tag{3.10}$$

The updated frequency and probe voltage are then applied to solve the bottom-level probe forced circuit again. The process is repeated until the probe current goes to zero where the solution is reached.

The Jacobian for the top-level probe equations is:

$$J_{probe} = \begin{bmatrix} \frac{\partial I_{probe}^c}{\partial V_{probe}} & \frac{\partial I_{probe}^c}{\partial \omega} \\ \frac{\partial I_{probe}^s}{\partial V_{probe}} & \frac{\partial I_{probe}^s}{\partial \omega} \end{bmatrix}
\tag{3.11}$$

It should be noted that the frequency is updated only at the top level where the bottom-level probe-forced circuit already converges and KCLs are satisfied for the circuit-probe combination. This results in an improved convergence.

### 3.4.2 Convergence Conditions and Challenges

The success of the two-level method, however, depends on 1) a close initial guess for the oscillation frequency and the probe voltage, and 2) the convergence of the bottom-level probe-forced circuit equations.

A pole-zero analysis can be used for the initial frequency guess. A curve tracking is used to get the initial guess for the probe voltage as shown in Fig. 3.8 where the curve of the probe current is tracked as a function of the probe voltage for a fixed frequency [7]. If the frequency used is the actual oscillation frequency, then at a certain probe voltage, the probe current will go to zero as expected. This voltage corresponds to the solution for the probe voltage. If the frequency used is close to the actual oscillation frequency, such as the frequency from a pole-zero

analysis, then there will be a local minimum. The corresponding voltage value is quite close to the probe voltage solution as shown in Fig. 3.8 and can be used as a good initial guess for the probe voltage. However, this scheme for finding an initial guess for the probe voltage fails for some high-Q oscillators as will be shown later.

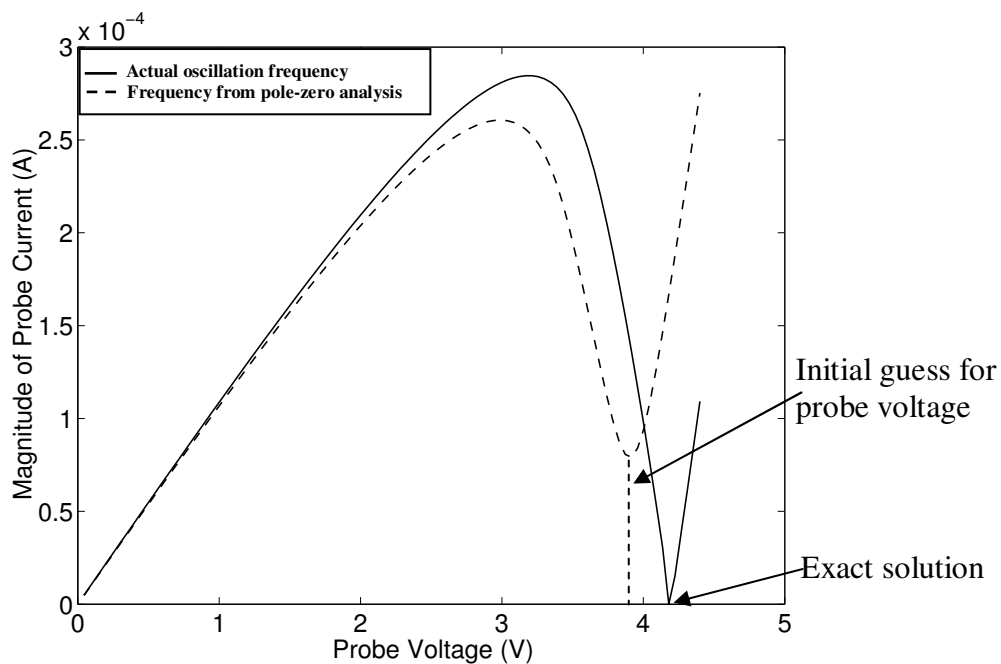


Figure 3.8: Probe current tracking curves for selecting an initial probe voltage. Use of the frequency from a pole-zero analysis provides a good initial guess for the probe voltage (minimum in the tracking curve).

With a good initial guess for the frequency and probe voltage, Newton's method can be applied to solve the top-level probe equations. However, the construction of the top-level Jacobian matrix needs the information from the

bottom-level Jacobian when the bottom-level equations have converged. Convergence of the bottom-level voltage-probe forced circuit can be a challenge for some highly nonlinear oscillators such as ring oscillators as shown later.

### **3.5 Summary**

In this chapter various oscillator structures and their operation are reviewed. Harmonic oscillators, ring oscillators and relaxation oscillators are discussed. The application of the frequency-domain harmonic balance method to oscillator simulation is introduced. The direct method of simply adding the frequency to the list of unknowns suffers from convergence problems. To overcome the convergence problems, a more robust probe technique is typically used. This technique is described along with its implementation by a two-level method. Conditions for convergence are also discussed in detail.

## 4. FREQUENCY-DOMAIN SIMULATION OF HIGH-Q OSCILLATORS

### 4.1 Introduction

Traditional time-domain steady state analysis is impractical for high-Q oscillators since a very large number of oscillator periods have to be simulated before the steady state is reached. Accelerated steady state analysis methods (in time or frequency domains) alleviate this problem [2].

Frequency-domain analysis using the harmonic balance method is particularly efficient for high-Q oscillators. The steady-state circuit waveforms can be directly obtained using a small number of harmonics because of the high-Q nature of the circuit. Furthermore, the harmonic balance method is more accurate than the time domain method for circuits with band-limited waveforms due to its exponential convergence nature. Efficiency and accuracy requirements make the frequency-domain harmonic balance method an ideal candidate for high-Q oscillator simulation.

The harmonic balance method has been successfully used for the simulation of oscillators using the concept of a periodic voltage probe [7]. However, high-Q oscillator simulation using the harmonic balance method is a difficult problem due to a small region of convergence. Prior research has focused on obtaining the region of convergence with two dimensional optimization procedures [37]. However, this procedure can be very expensive since it involves repeatedly solving many harmonic balance equations.

A detailed analysis in [8, 9] shows that a continuation method in conjunction with the voltage probe of [7] can be successfully used to simulate a high-Q oscillator. A multistage continuation approach for oscillator simulation using a Hopf bifurcation is also proposed in [10]. However, the specific details of the

continuation methods are not provided [8-10]. In this chapter, we explore the use of homotopy methods [11-12] for the steady-state simulation of high-Q oscillators in the frequency domain.

This chapter is organized as follows. The challenges for high-Q oscillator simulation in the frequency domain are introduced in Section 4.2. In Section 4.3 the theory of homotopy methods is reviewed. Then the homotopy method solver HOMPACT [11] is described in Section 4.4. Homotopy methods are applied to the frequency-domain simulation of high-Q oscillators and different embedding methods are given in Section 4.5. This chapter is summarized in Section 4.6.

## 4.2 Convergence Problems in High-Q Oscillators

As shown in the previous chapter, the two-level method requires a good starting point for the oscillation frequency and the probe voltage. A pole-zero analysis is commonly used for estimating the oscillation frequency. With this initial frequency, the probe current is tracked while stepping the probe voltage. For most circuits a local minimum is obtained and the corresponding probe voltage is then a good initial guess [7]. However, for high-Q oscillators such a minimum does not exist even when the initial oscillation frequency from a pole-zero analysis is sufficiently close to the exact solution as shown in Fig. 4.1. To see how small the region of convergence for a high-Q oscillator is, the probe current is tracked for different frequencies which are close to the actual oscillation frequency. From Fig. 4.1 we can see that a local minimum of the probe current is

obtained only for frequency initial guesses  $f$  that satisfy  $\left| \frac{f - f_0}{f_0} \right| \leq 0.005\%$ , where

$f_0$  is the oscillation frequency. This indicates that the region of convergence is extremely small and it is almost impossible for a user to specify a proper initial

guess for the frequency of oscillation. Without a proper initial guess for the probe frequency, an initial guess for the probe voltage cannot be determined and the two-level method will have convergence problems. For this reason, a method which does not require an initial guess for the probe voltage is needed for high-Q oscillator circuits. Homotopy methods with a proper embedding belong to this category as described in the next section.

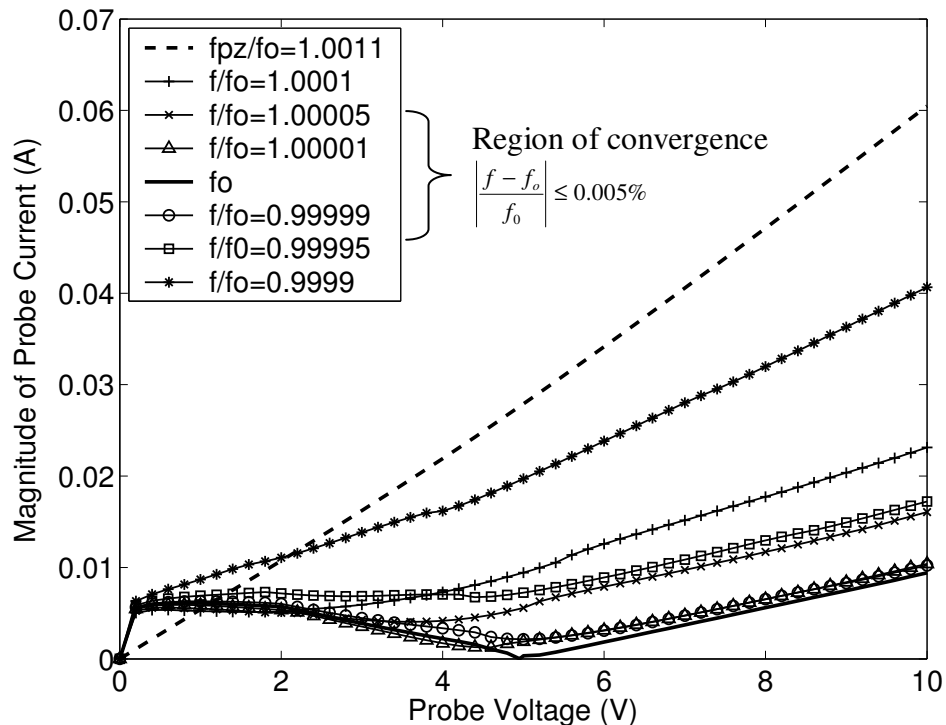


Figure 4.1: Probe current tracking curves.  $f_0$  is actual oscillation frequency,  $fpz$  is the frequency from the pole-zero analysis, and  $f$  is a guess for the oscillation frequency.

### 4.3 Theory of Homotopy Methods

Homotopy methods belong to the class of continuation methods where the homotopy parameter does not necessarily vary monotonically as the path from the

original solution to the final solution is followed. This is accomplished by making the continuation parameter a function of the path length [38]. The path length always increases while the continuation parameter may vary arbitrarily.

Consider the solution of a system of  $n$  nonlinear equations in  $n$  variables

$$F(x) = 0 \quad (4.1)$$

where  $F: R^n \rightarrow R^n$  is a smooth mapping. A homotopy function  $H(x, \lambda)$  is created by embedding a parameter  $\lambda$  which results in a system of equations of higher dimension

$$H(x, \lambda) = 0 \quad (4.2)$$

where  $H: R^n \times R \rightarrow R^n$ . For  $\lambda = 0$ ,  $H(x, 0) = G(x) = 0$  is an easy problem to solve, whereas for  $\lambda = 1$ ,  $H(x, 1) = F(x) = 0$  yields the solution of the original problem. The parameter  $\lambda$  is called the homotopy parameter. By following the solutions of  $H(x, \lambda) = 0$  as  $\lambda$  varies from 0 to 1, the solution to  $F(x) = 0$  is found and the solution trace is known as the zero curve.

The benefit of this approach is that the solution at a previous  $\lambda$  point can be used as a good initial guess for the current  $\lambda$  point. With this good initial guess only a few steps of Newton's method are needed to find the solutions for each  $\lambda$ . Provided that  $H(x, 0) = 0$  has a unique solution, the solution  $x$  is bounded along the zero curve and the homotopy path is bifurcation free, the homotopy method guarantees a reliable solution from an arbitrary starting point [11]. This characteristic makes homotopy methods extremely useful when an initial guess, required for a local Newton method, is not available or simply is too difficult to obtain.

The choice of the embedding function  $H(x, \lambda)$  is critical for the homotopy method to work robustly and efficiently [11-12]. There are two general ways to

embed a homotopy parameter. The first method is a natural parameter homotopy, where a system parameter is chosen and swept across a range of values, and, therefore, plays the role of the homotopy parameter  $\lambda$ . The most commonly used natural parameter homotopy in circuit simulation is the “source stepping”. However, natural homotopies are often prone to bifurcations of the homotopy path. The second method is an artificial parameter homotopy, where the homotopy parameter  $\lambda$  is embedded in the nonlinear equations and is not related to any system parameters. By proper construction of the artificial parameter homotopies, bifurcations and other singular and ill-conditioned behavior can be avoided.

#### ***4.3.1 Homotopy methods for DC operating point problem***

Homotopy methods have been used extensively for finding the dc operating points of “difficult-to-solve” nonlinear circuits [12-15]. In these applications, variations of homotopy methods have been constructed for the nonlinear equations describing transistor circuits or device models.

- **Fixed-point homotopy**

The fixed-point homotopy is based on the equation

$$H(x, \lambda) = \lambda F(x) - (1 - \lambda)G(x - a) \quad (4.3)$$

where a new parameter  $G \in R^n \times R^n$  is embedded. This homotopy represents an augmented circuit derived from the original circuit. A branch consisting of a conductance  $\frac{1-\lambda}{\lambda}G$  in series with a voltage source  $a_k$  is connected to every node.

At  $\lambda = 0$  the conductance goes to infinity and the voltage at each node is simply

forced by  $a_k$ . When  $\lambda = 1$ , the conductance equals to zero, the added branches are disconnected from the circuit and the original circuit is recovered.

- Variable-stimulus homotopy

The variable-stimulus homotopy is based on the equation

$$H(x, \lambda) = F(x, \lambda) - (1 - \lambda)G(x - a) \quad (4.4)$$

In this homotopy mapping, the node voltages of the nonlinear elements are multiplied by  $\lambda$ . So the homotopy starts from a linear circuit by setting all the voltages across the nonlinear elements to zero. The advantage of this embedding is that numerical overflows often encountered in exponential nonlinearities in p-n junctions are avoided. This homotopy converges faster to the desired solution than the fixed-point homotopy [12-13].

- Variable-gain homotopy

The variable-gain homotopy is designed specially for bipolar circuits, and is based on the equation

$$H(x, \lambda) = F(x, \lambda\alpha) - (1 - \lambda)G(x - a) \quad (4.5)$$

where  $\alpha$  is a column vector consisting of transistor forward and reverse current gains. When  $\lambda = 0$  the transistor current gain goes to zero, so the circuit only consists of resistors and diodes. Such a circuit has a unique and easy-to-solve dc operating point. The variable gain homotopy converges very fast for bipolar circuits [12-13].

- The BLHOM homotopy

The BLHOM homotopy is designed specially for MOSFET circuits [14]. A key feature of this homotopy is that it uses two  $\lambda$  parameters which are directly embedded into the MOSFET level one model

$$I_{ds} = \beta [v_{gs}'(v_{gb}, v_{db}, v_{sb}, \lambda_2)]^2 h(v_{db} - v_{sb}, \lambda_1) \quad (4.6)$$

$\lambda_1$  influences the drain-source driving-point characteristic whereas  $\lambda_2$  controls the transfer characteristics. At  $(\lambda_1, \lambda_2) = (0, 0)$ , there is no transfer characteristic (varying  $v_{gs}$  does not alter  $I_{ds}$ ), and the driving point characteristic is less sharper than that for the original MOSFET. The homotopy mapping starts from  $(\lambda_1, \lambda_2) = (0, 0)$  for which each MOS device becomes a two-terminal almost linear resistor, hence the circuit becomes easy to solve. This embedding method works well for large-scale MOSFET circuits.

#### 4.3.2 Homotopy methods for time-domain steady-state analysis of oscillators

Recently, homotopy methods have also been applied to the steady-state analysis of oscillators in the time domain combined with the shooting method [16-17] and the finite-difference method [18].

- Homotopy with shooting method

The original problem is

$$\begin{cases} x(0) - \Phi(x(0), 0, T) = 0 \\ x_i(0) - a = 0 \end{cases} \quad (4.7)$$

where  $x$  is the circuit state vector, including the voltages across the capacitors and currents through the inductors.  $\Phi$  is the state transition function which can be obtained by a regular transient analysis starting from the initial state  $x(0)$ .

$x_i(0) - a = 0$  is an additional constraint for an oscillator circuit to isolate the solution.

The homotopy map is based on the equation

$$\begin{cases} \lambda(x(0) - \Phi(x(0), 0, T)) + (1 - \lambda)(x(0) - x_{init}) = 0 \\ \lambda(x_i(0) - a) + (1 - \lambda)(T - T_{init}) = 0 \end{cases} \quad (4.8)$$

where  $x_{init}$  is the initial value for the state variables and  $T_{init}$  is the initial period value from a pole-zero analysis. By sweeping  $\lambda$  from 0 to 1, the problem goes from an easy to solve initial value problem to the original periodic boundary value problem.

- Homotopy with finite-difference method

The original problem is

$$F(x) = I(x) + \nabla Q(x) = 0 \quad (4.9)$$

where  $x$  is the circuit waveform vector,  $I$  is the contribution from the resistive part,  $Q$  is the contribution from the reactive part and  $\nabla$  represents the discretized time derivative. The homotopy technique sweeps from an initial value problem ( $\lambda = 0$ ) to a periodic boundary value problem ( $\lambda = 1$ ):

$$\begin{aligned} F(x, \lambda_1, \omega) &= I(x) + \widehat{\nabla} Q(x) + \overline{\nabla} Q(\widehat{x}) = 0 \\ \widehat{x} &= \lambda_1 x + (1 - \lambda_1) x_0 \end{aligned} \quad (4.10)$$

where  $\widehat{\nabla}$  and  $\overline{\nabla}$  are block lower triangular and strictly block upper triangular matrices, respectively, and  $\nabla = \widehat{\nabla} + \overline{\nabla}$ . This homotopy mapping has been applied to solve different oscillators where Newton's method fails.

#### 4.4 Homotopy Method Solver: HOMPACK

HOMPACK is a large collection of Fortran subroutines for solving various nonlinear systems of equations by homotopy methods [11]. The algorithms in HOMPACK are based on “artificial-parameter generic homotopies”. While Newton’s method only has a local convergence, HOMPACK is globally convergent with probability one under mild assumptions. These assumptions are

- A unique solution at  $\lambda=0$ .
- A bifurcation free zero curve.
- A bounded solution without rapid oscillation along the zero curve.

At the end of zero curve (when  $\lambda=1$ ) singularities may be encountered. This happens precisely when the original problem is singular at the solution. For some mild singularities, the homotopy method can remain nonsingular at the solution, but in the general case this is not so.

There are three different algorithms in HOMPACK:

- Fixpdf: ordinary differential equation-based method.
- Fixpnf: augmented Jacobian method.
- Fixpqf: normal flow algorithm.

Among them, the fixpdf algorithm is the most robust but it generally takes more  $\lambda$  steps and so it is computationally more expensive. It is difficult to predict which algorithm will be the best for a given problem.

HOMPACK divides the problem into three subdivisions:

- Fixed-point problem

The equation  $x = F(x)$  is solved by following the zero curve of the homotopy map

$$H(x, \lambda) = (1 - \lambda)(x - a) + \lambda(x - F(x)) \quad (4.11)$$

starting from  $\lambda = 0$  and  $x = a$ . The curve is parameterized by arc length  $s$ .

- Zero-finding problem

The equation  $F(x) = 0$  is solved by following the zero curve of the homotopy map

$$H(x, \lambda) = (1 - \lambda)(x - a) + \lambda F(x) \quad (4.12)$$

starting from  $\lambda = 0$  and  $x = a$ . The curve is also parameterized by arc length  $s$ .

- Curve-tracking problem

The curve-tracking problem deals with an arbitrary embedding of  $\lambda$ . The homotopy map  $H(a, \lambda, x)$  is assumed to satisfy

$$\text{rank}\left[\frac{\partial H(a, \lambda, x)}{\partial \lambda}, \frac{\partial H(a, \lambda, x)}{\partial x}\right] = N \quad (4.13)$$

for all points  $(\lambda, x)$  such that  $H(a, \lambda, x) = 0$ . It is further assumed that

$$\text{rank}\left[\frac{\partial H(a, \lambda, x)}{\partial x}\right] = N \quad (4.14)$$

with  $a$  fixed. The zero curve of  $H(a, \lambda, x)$  starting from  $\lambda = 0$  and  $x = x_0$  is tracked until  $\lambda = 1$  by solving the ordinary differential equation  $\frac{\partial H(a, \lambda(s), x(s))}{\partial s} = 0$  where  $s$  is the arc length along the zero curve. Also the

homotopy map  $H(a, \lambda, x) = 0$  is assumed to be constructed such that  $\frac{\partial \lambda(0)}{\partial s} = 0$ .

For the fixed-point and zero-finding problems, the user must supply a subroutine  $f(x, v)$  which evaluates  $F(x)$  at  $x$  and returns the value to vector  $v$ , and a subroutine  $ffac(x, v, k)$  which returns in  $v$  the  $k$ th column of the Jacobian matrix of  $F(x)$  evaluated at  $x$ .

For the curve tracking problem, the user must supply a subroutine  $rho(a, \lambda, x, v)$  which evaluates  $H(a, \lambda, x)$  at  $(a, \lambda, x)$  and returns the value to vector  $v$ , a subroutine  $rhoa(a, \lambda, x, par, ipar)$  which given  $(\lambda, x)$  returns a parameter vector in  $a$  such that  $H(a, \lambda, x) = 0$ , and a subroutine  $rhojac(a, \lambda, x, v, k, par, ipar)$  which returns in  $v$  the  $k$ th column of the  $N \times (N + 1)$  Jacobian matrix  $[\frac{\partial H(a, \lambda, x)}{\partial \lambda}, \frac{\partial H(a, \lambda, x)}{\partial x}]$  evaluated at  $(a, \lambda, x)$ .

#### 4.5 Homotopy Formulations for Frequency-Domain Simulation of Oscillators

As has been shown in Section 4.1, obtaining an initial guess for the probe voltage for some high-Q oscillators is difficult. For this reason, Newton's method can't be used to solve the top-level probe equations. The application of a homotopy method is described in this section.

The original equations are the top-level probe equations as shown in Eq. (3.10). In order to apply a homotopy map, Eq. (3.10) first needs to be modified by dividing with the probe voltage as shown in Eq. (4.15). The purpose of doing so is to isolate the real solution from the trivial DC solution of Eq. (3.10) which the homotopy map is more easily attracted to.

$$\begin{aligned}\frac{I_{probe}^c(V_{probe}, \omega)}{V_{probe}} &= 0 \\ \frac{I_{probe}^s(V_{probe}, \omega)}{V_{probe}} &= 0\end{aligned}\tag{4.15}$$

A homotopy map is then applied to the above modified top-level probe equations.

$$\begin{aligned}\lambda \frac{I_{probe}^c(V_{probe}, \omega)}{V_{probe}} + (1-\lambda)g_1(V_{probe} - V_{init}) &= 0 \\ \lambda \frac{I_{probe}^s(V_{probe}, \omega)}{V_{probe}} + (1-\lambda)g_2(\omega - \omega_{init}) &= 0\end{aligned}\tag{4.16}$$

where  $V_{init}$  and  $\omega_{init}$  are the initial values for the probe voltage and frequency, and  $g_1$  and  $g_2$  are scaling factors. The typical value for  $g_1$  is  $10^{-4}$  and  $g_2$  is chosen such that both terms in Eq. (4.16) are of a similar magnitude depending on the frequency of oscillation. From Eq. (4.16) we can see that by sweeping from  $\lambda = 0$  to  $\lambda = 1$ , the homotopy map goes gradually from an easy to solve forced circuit problem to a hard to solve problem, i.e., the original oscillator problem.

A Pierce crystal oscillator from [8, 9] is shown in Fig. 4.2 and used to evaluate the above homotopy algorithm. The crystal  $Q$  is  $2.5 \times 10^4$ . The circuit has two poles ( $1.6774645 \times 10^4 \pm j6.289348 \times 10^7$ ), and the initial guess for the oscillation frequency is set to 10.008745MHz correspondingly. The voltage probe is placed at the high-impedance collector node of the BJT. Figs. 4.3 and 4.4 show the solution traces with the initial probe voltage starting from a probe voltage equal to the DC operating point value and 1mV, respectively. The traces are from the FIXPDF algorithm. Similar traces are obtained with the FIXPQF and FIXPNF algorithms.

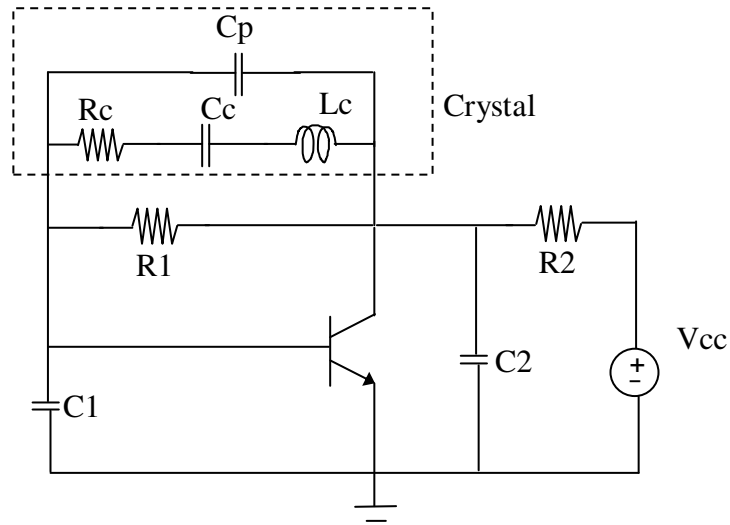


Figure 4.2: Circuit schematic of the Pierce oscillator.  $R1=100\text{K}\Omega$ ,  $R2=2.2\text{K}\Omega$ ,  $C1=100\text{pF}$ ,  $C2=100\text{pF}$ ,  $Cp=25\text{pF}$ ,  $Cc=99.5\text{fF}$ ,  $Rc=6.4\Omega$ ,  $Lc=2.55\text{mH}$ ,  $Vcc=12\text{V}$ ,  $\beta=100$  for the BJT.

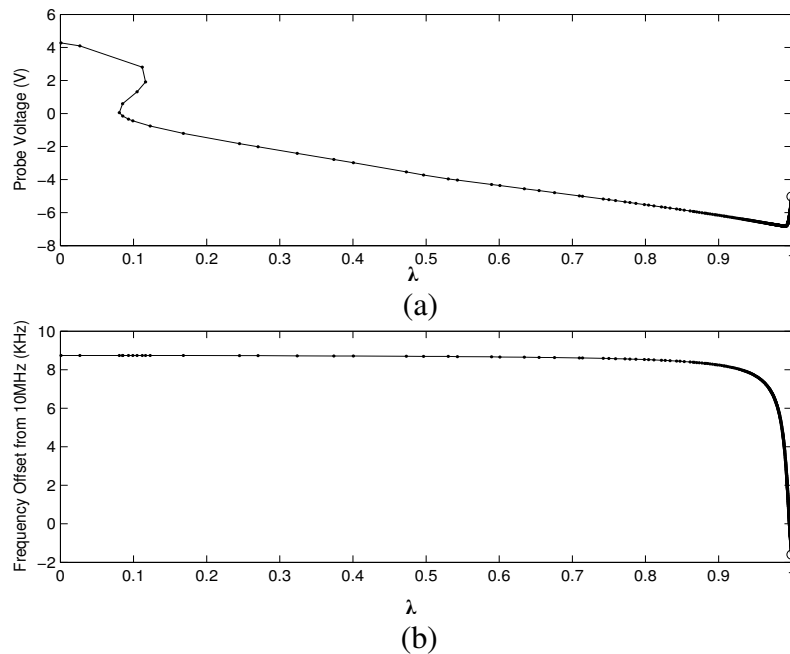


Figure 4.3: Solution traces for the Pierce oscillator with the initial probe amplitude equal to the DC solution. (a) Probe voltage as a function of  $\lambda$ . (b) Oscillation frequency as a function of  $\lambda$ .

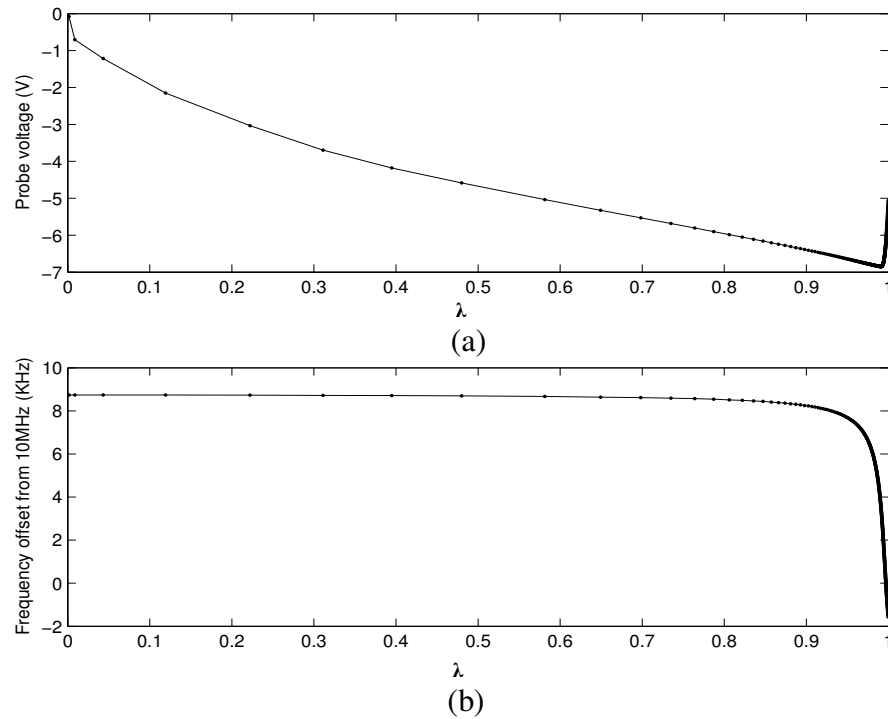


Figure 4.4: Solution traces for the Pierce oscillator with the initial probe amplitude equal to 1mV. (a) Probe voltage as a function of  $\lambda$ . (b) Oscillation frequency as a function of  $\lambda$ .

From Figs. 4.3 and 4.4 we can see the progress of the probe voltage and oscillation frequency as a function of the embedding parameter  $\lambda$ . For the curve starting from the DC operating point value, the probe voltage tends to go to the DC solution (a probe amplitude of 0V), but the modified equations handle this situation and the probe voltage converges to a negative value that is a valid solution. For the curve starting from a small value, the tracking curve goes to the periodic steady-state solution directly since the original probe equations have been effectively modified to isolate the trivial DC solution.

The problem with the embedding in Eq. (4. 16) is that it converges slowly although it is robust. In this particular case, more than a thousand steps (several

thousand Jacobian evaluations) were needed to obtain the solution. A closer examination of the solution traces reveals the possible causes. The probe voltage and frequency are two different parameters and embedding them with the same parameter  $\lambda$  is not the most efficient approach. Furthermore, from Fig. 4.3 we see that from  $\lambda = 0$  to about  $\lambda = 0.7$ , the change in frequency is very small, but the probe voltage progresses quickly even with turning points. After  $\lambda = 0.7$ , the solution trace for frequency shows a change and the tracking takes several steps. Fig. 4.4 shows the same trend. This suggests that the tracking for the voltage and the oscillation frequency should be decoupled by using two different embedding parameters. For this reason,  $\lambda_1$  is used for embedding the probe voltage and  $\lambda_2$  is used for embedding the oscillation frequency. Then a revised algorithm is obtained as shown in Fig. 4.5.

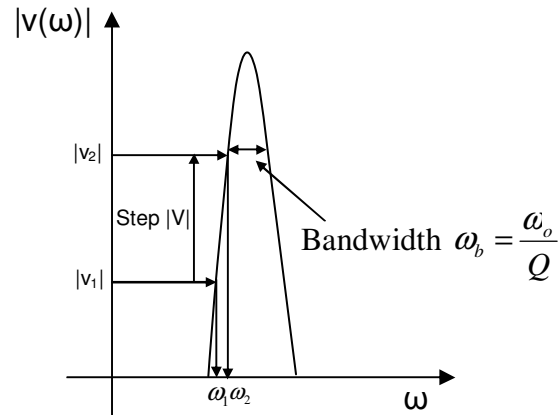
While ( $\lambda_1 \neq 1$ ) do {

1. For each  $\lambda_1$  (fixed probe voltage), track  $\lambda_2$  from 0 to 1.
 
$$\lambda_2 \frac{I_{probe}^s(V_{probe}, \omega)}{V_{probe}} + (1 - \lambda_2) g_2(\omega - \omega_{init}) = 0$$
2. When  $\lambda_2$  equals 1 (fixed frequency), step  $\lambda_1$ .
 
$$\lambda_1 \frac{I_{probe}^c(V_{probe}, \omega)}{V_{probe}} + (1 - \lambda_1) g_1(V_{probe} - V_{init}) = 0$$

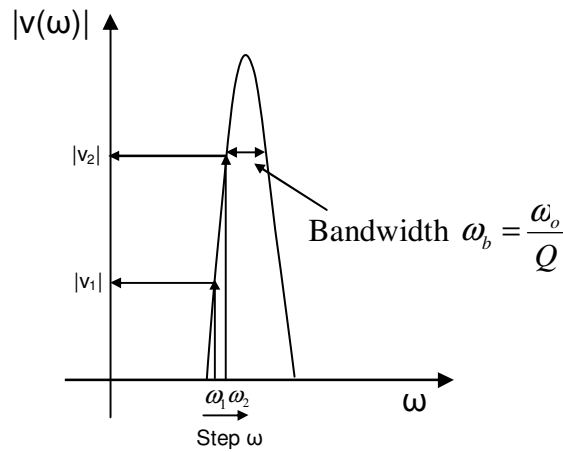
}

Solution is obtained for  $\lambda_1=1$ .

Figure 4.5: Algorithm 1: A two-parameter embedding homotopy algorithm.



(a)



(b)

Figure 4.6: The solution tracking process in a high-Q resonator. (a) The voltage in the outer loop and frequency in the inner loop. (b) The frequency in the outer loop and voltage in the inner loop.

In this algorithm  $\lambda_1$  (probe voltage) and  $\lambda_2$  (frequency) are solved iteratively.  $\lambda_1$  (probe voltage) is tracked in the outer loop while  $\lambda_2$  (frequency) is tracked in the inner loop. The reason for this ordering can be seen from the tracking process

in a high-Q resonator as shown in Fig. 4.6. From Fig. 4.6(a) we can see if the voltage is in the outer loop, at a fixed voltage  $V_1$  we will get the frequency solution  $\omega_1$ , then the voltage is stepped to a new value  $V_2$  using the embedding function as in Fig. 4.5. For this new voltage  $V_2$ , we need to solve for the corresponding  $\omega_2$ . As seen from Fig. 4.6(a), the frequency corresponding to voltage  $V_1$  serves as a good initial guess since it is quite close to  $\omega_2$ . However, if the process is reversed as in Fig. 4.6(b) where the frequency is in the outer loop and the voltage is in the inner loop, a very small step in  $\omega$  (from  $\omega_1$  to  $\omega_2$ ) will introduce a large change in the voltage (from  $V_1$  to  $V_2$ ). In this case,  $V_1$  is no longer a good initial guess for the new solution  $V_2$ <sup>1</sup>.

The globally convergent algorithms in [11] are based on a single homotopy parameter  $\lambda$ . The above algorithm is used with HOMPACK by switching the two embedding parameters. This algorithm provides a significant speed up even though  $\lambda_1$  and  $\lambda_2$  are solved iteratively. This algorithm can be further modified by noting that for a small value of the initial probe voltage (for starting the homotopy curve tracking), the oscillation frequency estimated by a linear pole-zero analysis serves as a very good initial guess. Therefore, a homotopy mapping to track the frequency is not necessary and one can simply use a Newton method in Step 1 of Algorithm 1. By doing so, the modified algorithm can be made more efficient since the homotopy method is generally more expensive than the Newton method. In addition, only one embedding parameter is needed which makes the implementation much easier. The corresponding algorithm, Algorithm 2, is given in Fig. 4.7.

---

<sup>1</sup> For high Q resonators, the voltage changes significantly for a small shift in frequency.

The new algorithms have been tested on different high-Q and moderate Q oscillators to demonstrate their convergence performance. The results are summarized in Chapter 7.

The probe voltage starts from a small value.

While ( $\lambda \neq 1$ ) do {

3. For each  $\lambda$  (fixed probe voltage), solve

$$I_{probe}^s(\omega) = 0$$

4. Step  $\lambda$

$$\lambda \frac{I_{probe}^c(V_{probe}, \omega)}{V_{probe}} + (1 - \lambda) g_1(V_{probe} - V_{init}) = 0$$

}

Solution is obtained for  $\lambda=1$ .

Figure 4.7: Algorithm 2: Modified embedding algorithm for high-Q oscillator simulation.

#### 4.6 Summary

In this chapter globally convergent homotopy methods have been applied to address the frequency-domain simulation of high-Q oscillators. The basic theory of homotopy methods and its application to DC operating points and time-domain steady-state oscillator simulation are reviewed. A brief description of the homotopy method solver, HOMPACT, is also given. Different embedding techniques have been proposed for frequency-domain high-Q oscillator simulation and an efficient and robust algorithm is identified.

## 5. FREQUENCY-DOMAIN SIMULATION OF HIGHLY NONLINEAR RING OSCILLATORS

### 5.1 Introduction

All previous work using the harmonic balance method for oscillator simulation has focused on LC oscillators which have near sinusoidal waveforms [7-10, 19]. Some of these techniques can be applied to simulate ring oscillators, but due to the highly nonlinear nature of these circuits, the simulation fails to converge. The mechanism of divergence for ring oscillators is different from that of high-Q oscillators. Ring oscillators have a low Q and the solution of highly nonlinear circuit equations is a problem rather than the initial guess for the probe frequency and voltage.

Commercially available harmonic balance simulators can only simulate highly nonlinear ring oscillators using results from a time-domain transient analysis as an initial guess. This approach, however, constrains the simulation of ring oscillators in a RF system where transient analysis is no longer efficient when mixer circuits are present. In this chapter, two new algorithms for robust simulation of ring oscillators are proposed.

This chapter is organized as follows. The challenges in ring oscillator simulation in the frequency domain are introduced in Section 5.2. A phase relationship for ring oscillators is identified in Section 5.3. By taking advantage of the ring oscillator phase relationship, two new methods for frequency-domain ring oscillator simulation are proposed. A single-delay cell method is described in Section 5.4 and a multiple-probe method is discussed in Section 5.5. This chapter is summarized in Section 5.6.

## 5.2 Convergence of Harmonic Balance Methods for Ring Oscillators

A comparison is made between the performance of the traditional harmonic balance method (HB) in Eq. (3.6), the continuation method of [8] (Cont1), the modified continuation method of [9] (Cont2) and the two-level method of [7] for different stage ring oscillators with a basic inverter cell (Fig. 5.1 (a)). The BSIM3 MOSFET model is used for all MOS devices. The traditional harmonic balance method and continuation method 1 (Cont1) failed after 300 iterations for all cases. The modified continuation method (Cont2) worked only for the first case. However, it is computationally much more expensive and less robust than the two-level method for ring oscillator simulation.

Table 5.1: Convergence performance comparison of different harmonic balance methods for ring oscillator simulation. × denotes no convergence in 300 iterations.

# stage	#Freq for HB Analysis	Freq (GHz)	# Iterations			
			HB	Cont1	Cont2	2-level
3	16	3.25	×	×	187	23
5	32	1.95	×	×	×	38
7	64	1.4	×	×	×	43

Although the two-level method is more robust than the continuation method for ring oscillator simulation, its convergence is still very sensitive to the initial guess. For some circuits the initial frequency guess must be within 1% of the oscillation frequency to reach convergence. Other circuits do not converge even when the exact oscillation frequency and probe voltage are given as the initial

guess. This is illustrated with results summarized in Table 5.2. In this table,  $|\Delta f|/f_{osc}$ ,  $|\Delta V_{probe}|/V_{osc}$  are the errors of the initial guess relative to the solution for the frequency and probe voltage, respectively.

Table 5.2: Convergence properties of different ring oscillator circuits.  $\times$  denotes no convergence under exact initial guess for oscillation frequency and probe voltage.

Oscillator circuit	Circuit 1	Circuit 2	Circuit 3	Circuit 4
Delay cell (Fig. 5.1)	(a)	(b)	(c)	(d)
# Stages	9	21	3	5
$ \Delta f /f_{osc}$	$\times$	1%	$\times$	1%
$ \Delta V_{probe} /V_{osc}$	$\times$	5%	$\times$	5%

A close examination of the results, for ring oscillators for which the simulation always fail, reveals convergence problems in the solution of the bottom-level voltage-probe forced circuit. A circuit waveform (the cosine part of the first harmonic of a node voltage) during the Newton iterative process from Circuit 3 is shown in Fig. 5.2. From Fig. 5.2 (a) we can see that the circuit waveform diverges even with a very small damping factor for the Newton method. To overcome this problem, voltage and current thresholds can be set, but from Fig. 5.2 (b) we see that the circuit waveform oscillates between these thresholds and fails to converge.

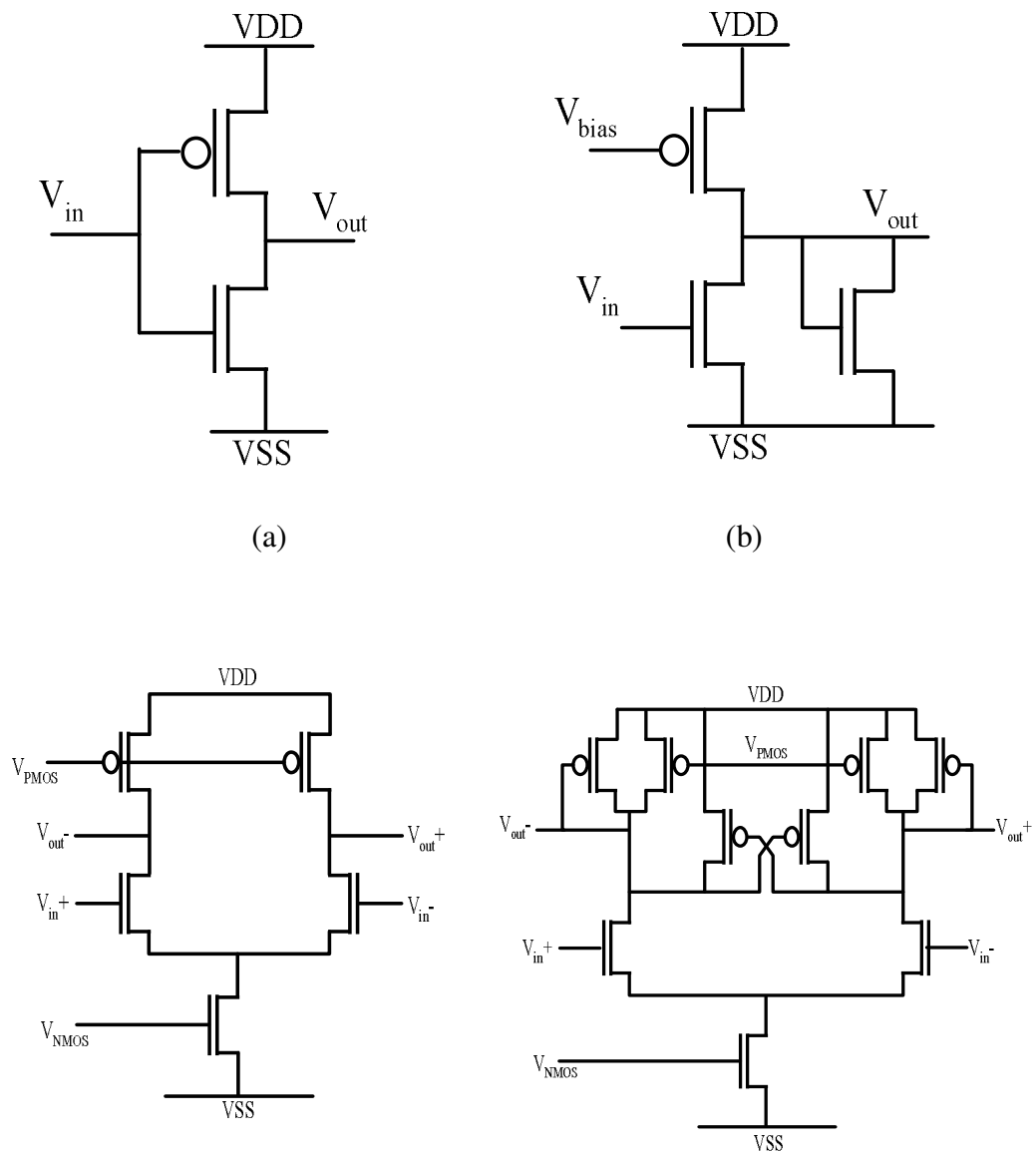
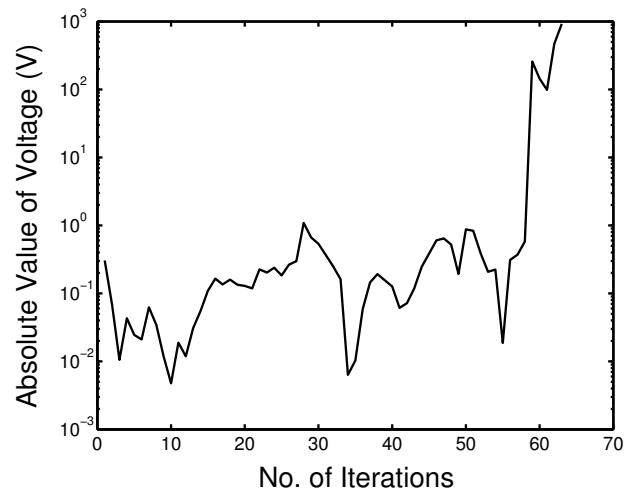
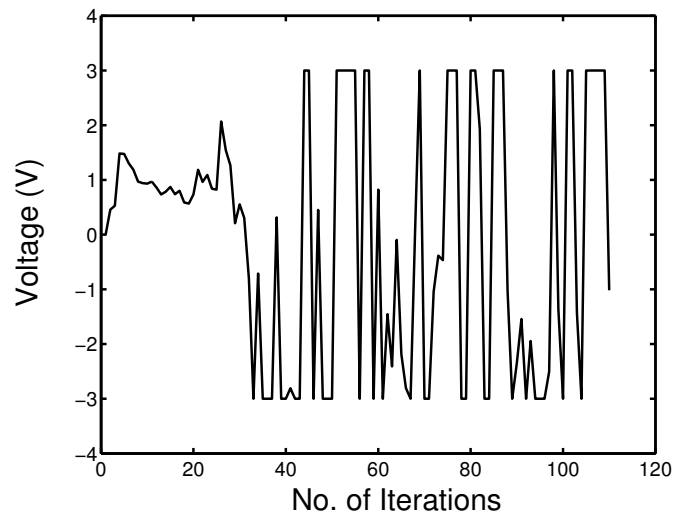


Figure 5.1: Ring oscillator delay cells. (a) Basic delay cell. (b) Current starved delay cell. (c) Vanilla delay cell. (d) Cross-coupled load delay cell [39].



(a)



(b)

Figure 5.2: Circuit waveform during the Newton iterative process. (a) Use of a small damping factor. (b) Adaptive damping with voltage/current thresholds.

The use of a homotopy method at the bottom-level has been investigated. The divergence in the ring oscillator simulation comes from the nonlinear active devices. So an embedding function that starts from only linear capacitances or linear capacitances and resistances has been tried. However, this approach did not give a good performance.

When a voltage source with the exact oscillation waveform at a node is used to force the ring oscillator circuit at that node, the circuit converges readily. This suggests that besides the high nonlinearity of the circuit, the manner in which the ring oscillator circuit is converted to a forced circuit also plays a critical role in the convergence performance.

Based on the above observations two new approaches are proposed for robust ring oscillator simulation. The first approach relies on a decrease in the number of nonlinear devices. The second approach uses a more effective forcing function. Both approaches exploit the periodic structure of ring oscillators.

### 5.3 Ring Oscillator Phase Relationships

Ring oscillators have a periodic structure, whereby the waveforms at the different nodes differ in phase by multiples of  $2\pi/m$ , where  $m$  is the number of the stages in the oscillator [40]. The explicit phase shift relationship between the input and output nodes of each delay cell can be seen from the time domain waveforms of a five-stage ring oscillator as shown in Fig. 5.3. In this particular case, the input and output differ in phase by  $\frac{6\pi}{5}$  ( $216^\circ$ ).

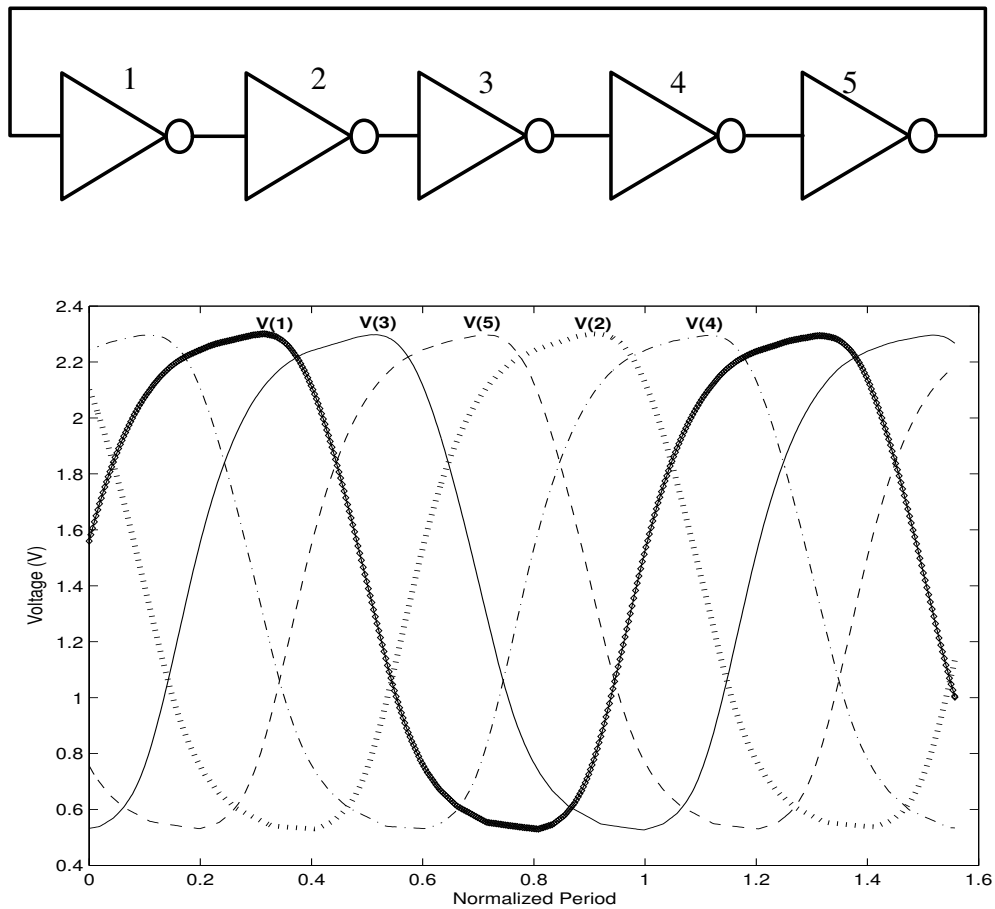


Figure 5.3: Five-stage ring oscillator waveform.

A general relationship for the phase shift of each delay cell is now derived. Recall that the period of oscillation for a ring oscillator is given by [35, 40]

$$T = 2m\tau_d \quad (5.1)$$

where  $\tau_d$  is the time delay of the delay cell. From Eq. (5.1), the time delay  $\tau_d$  corresponds to a phase shift of  $\pi/m$  radians. Since the inverting delay cell

contributes an additional phase shift of  $\pi$ , the phase delay for each inverting cell can be expressed as

$$\theta = \left(\frac{m+1}{m}\right)\pi \quad (5.2)$$

The phase relationship for a three-stage ring oscillator is shown in Fig. 5.4 which pictorially shows the above derivation. From Eq. (5.2) the total phase shift of a  $m$  stage ring oscillator will be  $(m+1)\pi$  when  $m$  is an odd number. If  $m$  is an even number, and noting that the last stage of the ring oscillator is non-inverting, the total phase shift is  $m\pi$  instead. In both cases, the total phase shift is a multiple of  $2\pi$  which guarantees a positive feedback.

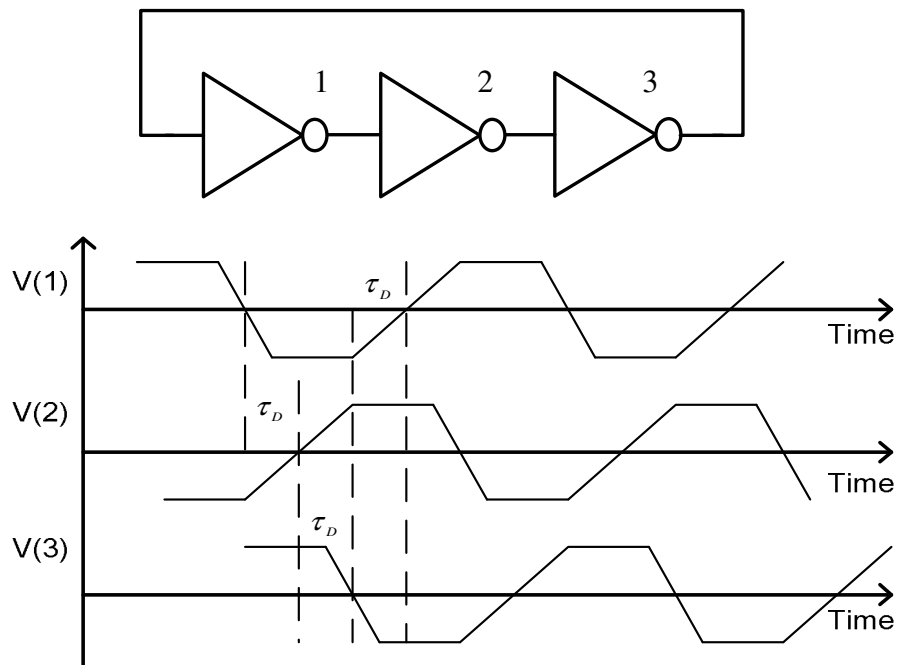


Figure 5.4: Phase relationship for a three-stage ring oscillator.

Based on the above observation we have the input-output voltage (current) phase relationship of a single-ended ring oscillator delay cell as

$$X_{out}^k = X_{in}^k e^{-jk\theta} \quad (5.3)$$

where  $X$  is the frequency-domain circuit waveform (complex vector),  $k$  is the harmonic order, and  $\theta$  is the phase relationship given in Eq. (5.2). For differential ring oscillators, this relationship holds for each half circuit, while the phase difference between the two half circuits is simply  $\pi$ .

## 5.4 Single-delay Cell Method

The single-delay cell method for ring oscillator simulation using the harmonic balance method recognizes the structure of the oscillator assuming all cells are identical. The phase relationships between the individual delay cells derived in the previous section are used to simulate a single-delay cell and determine the periodic steady state of the oscillator.

### 5.4.1 Single-delay Cell Equivalent Circuit

The basic idea behind the single-delay cell method is that one delay cell as well as the information about the number of stages gives enough information about the operation of the ring oscillator circuit. Therefore, instead of simulating the complete ring oscillator circuit, we can simplify the simulation to that of a single-delay cell equivalent circuit as shown in Fig. 5.5. The delay element gives the phase relationship between the input-output waveforms according to Eq. (5.3), which is a function of the number of stages as shown in Eq. (5.2).

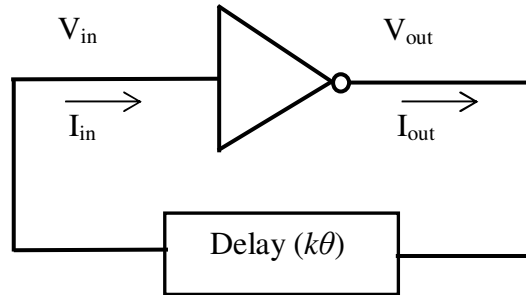


Figure 5.5: Single-delay cell equivalent circuit for ring oscillator simulation.

For differential ring oscillators, this relationship holds for each half circuit, while the phase difference between the two half circuits is simply  $\pi$ . The harmonic balance method, being a frequency-domain method, can handle the phase delay elements easily and efficiently. With a reduction in the number of nodes in the circuit, the simulation is considerably sped up. Furthermore, the convergence is also improved since fewer nonlinear devices are included in the simulation.

#### 5.4.2 Matrix Formulation for Harmonic Balance Method

The input and output voltage/current complex vectors can be expressed in rectangular coordinates as

$$\begin{aligned} X_{out}^k &= x_{out,c}^k + jx_{out,s}^k \\ X_{in}^k &= x_{in,c}^k + jx_{in,s}^k \end{aligned} \tag{5.4}$$

Substituting Eq. (5.4) into Eq. (5.3) we see that



### 5.4.3 Modified Voltage Probe Method

The voltage probe is used to convert the single-delay cell into a forced equivalent circuit. At  $f=f_{osc}$ , the input of the delay cell is driven with a voltage probe, and the input-output current still satisfy the relationship as in Eq. (5.3). This is expressed as a CCCS in the circuit schematic of Fig. 5.6. For frequencies  $f \neq f_{osc}$ , the circuit is the same as that in Fig. 5.5. The solution is obtained when the input-output voltages at the fundamental frequency satisfy Eq. (5.3).

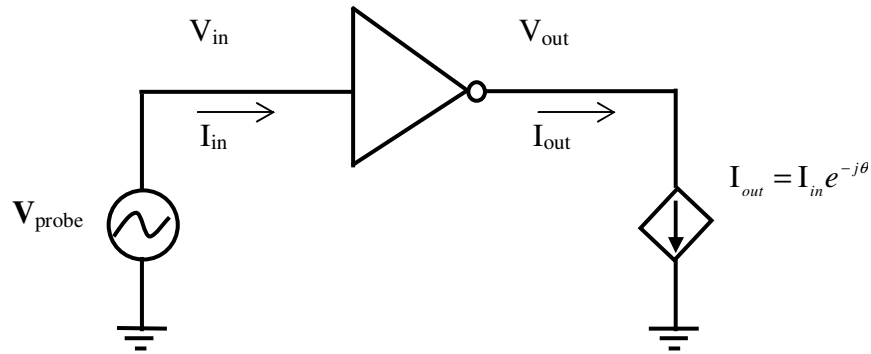


Figure 5.6: Single-delay cell equivalent circuit with a voltage probe at  $f = f_{osc}$ .

### 5.4.4 Solution by Newton's Method

The circuit is now solved with a two-level method. The first level of the two-level method solves the harmonic balance equations of the voltage probe forced circuit.

$$\begin{bmatrix} J_M & -e_i^c(1) & -e_i^s(1) \\ e_{in}^c(1)^T & 0 & 0 \\ e_{in}^s(1)^T & 0 & 0 \end{bmatrix} \begin{bmatrix} X^{(j+1)} \\ \Delta V_c \\ \Delta V_s \end{bmatrix} = \begin{bmatrix} RhsF^{(j)} \\ V_{probe} \\ 0 \end{bmatrix} \quad (5.7)$$

$$\begin{aligned}
\Delta V_c &= -\cos \theta V_{in,c}^1 - \sin \theta V_{in,s}^1 + V_{out,c}^1 \\
\Delta V_s &= \sin \theta V_{in,s}^1 - \cos \theta V_{in,c}^1 + V_{out,s}^1
\end{aligned}
\tag{5.8}$$

where  $J_M$  is the modified harmonic balance Jacobian with the branch constitutive equations stamped according to Eq. (5.6).  $e_{in}^c(1)$  ( $e_{in}^s(1)$ ) is the unit vector that selects the cosine (sine) part of the first harmonic of the node to which the probe is attached.  $e_i^c(1)$  ( $e_i^s(1)$ ) is the unit vector that selects the branch constitutive equations in Eq. (5.6) to open the voltage delay circuit at the fundamental frequency.  $V_{in,c}^1$  ( $V_{in,s}^1$ ) is the cosine (sine) part of the first harmonic of the input voltage.  $V_{out,c}^1$  ( $V_{out,s}^1$ ) is the cosine (sine) part of the first harmonic of the output voltage.

The second level solves the probe equations:

$$\begin{aligned}
\Delta V_c(V_{probe}, \omega) &= 0 \\
\Delta V_s(V_{probe}, \omega) &= 0
\end{aligned}
\tag{5.9}$$

The Jacobian for this set of equations is:

$$J_{probe} = \begin{bmatrix} \frac{\partial \Delta V_c(V_{probe}, \omega)}{\partial V_{probe}} & \frac{\partial \Delta V_c(V_{probe}, \omega)}{\partial \omega} \\ \frac{\partial \Delta V_s(V_{probe}, \omega)}{\partial V_{probe}} & \frac{\partial \Delta V_s(V_{probe}, \omega)}{\partial \omega} \end{bmatrix}
\tag{5.10}$$

This 2x2 Jacobian can be obtained by a simple computation using information from the first-level solution.

The frequency-domain nonlinear equations for the circuit-probe combination,  $G$ , can be expressed as:

$$G(X_A, \omega) = 0
\tag{5.11}$$

where  $X_A$  is the vector of the circuit unknowns, and  $\Delta V_c$  and  $\Delta V_s$ . The sensitivity with respect to  $V_{probe}$  and  $\omega$  can then be computed as:

$$\begin{aligned} \frac{\partial G}{\partial X_A} \frac{\partial X_A}{\partial V_{probe}} &= - \frac{\partial G}{\partial V_{probe}} \\ \frac{\partial G}{\partial X_A} \frac{\partial X_A}{\partial \omega} &= - \frac{\partial G}{\partial \omega} \end{aligned} \quad (5.12)$$

where  $\frac{\partial G}{\partial X_A}$  is the augmented Jacobian in Eq. (5.7). All entries of the 2x2 Jacobian matrix in Eq. (5.10) can be extracted from the solution of Eq. (5.12).

#### 5.4.5 Differential Ring Oscillator Simulation

For differential ring oscillators, the voltage probe is added to the circuit at the oscillation frequency differentially. By doing this, the phase constraints are automatically forced for the two half circuits. Each half circuit has the phase relationship as in the single-ended oscillator. The equivalent schematic of the circuit in the frequency domain is shown in Figs. 5.7 and 5.8.

To effectively open the voltage delay block for both half circuits, we observe that  $\Delta V_c$  and  $\Delta V_s$  for the two half circuits have a phase difference of  $\pi$ . Using this information, the Jacobian can be constructed as:

$$\begin{bmatrix} J_M & -I_i^c(1) & -I_i^s(1) \\ I_{in}^c(1)^T & 0 & 0 \\ I_{in}^s(1)^T & 0 & 0 \end{bmatrix} \begin{bmatrix} X^{(j+1)} \\ \Delta V_c \\ \Delta V_s \end{bmatrix} = \begin{bmatrix} RhsF^{(j)} \\ V_{probe} \\ 0 \end{bmatrix} \quad (5.13)$$

where  $I_i^c(1)$  ( $I_i^s(1)$ ) is of the form  $[\dots 1 \dots -1 \dots]^T$ , which selects the branch constitutive equations in Eq. (5.6) to open the voltage delay circuit at the

fundamental frequency for each half circuit.  $I_{in}^c(1)$  ( $I_{in}^s(1)$ ) is also of the form  $[\dots 1 \dots -1 \dots]$  where the cosine (sine) part of the first harmonic of the differential input nodes to which the probe is attached are selected.

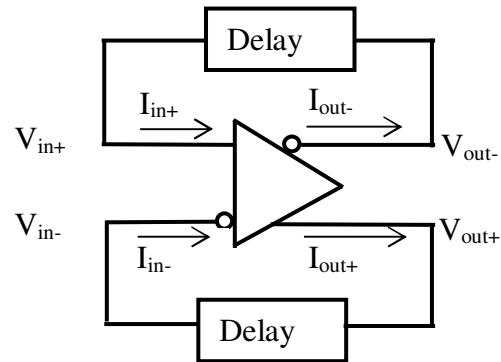


Figure 5.7: Single-delay cell equivalent circuit for a differential ring oscillator at  $f \neq f_{osc}$ .

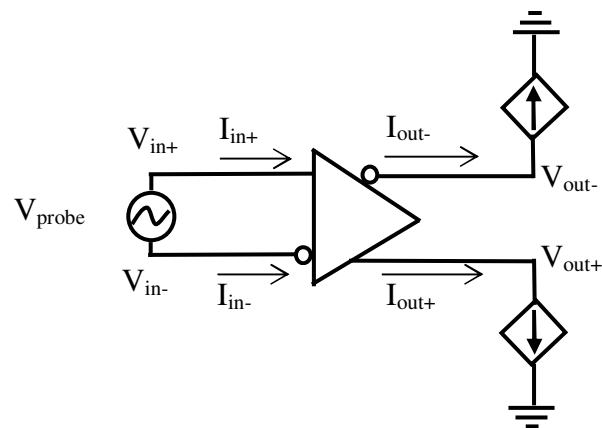


Figure 5.8: Single-delay cell equivalent circuit with a voltage probe for the differential ring oscillator at  $f = f_{osc}$ .

#### 5.4.6 *Limitation*

The proposed single-delay cell method assumes that all the oscillator cells are identical and cannot be used when large mismatches between cells need to be accounted for. More work needs to be done on extensions of this work to non-identical delay cells.

### 5.5 **Multiple-probe Method**

The multiple-probe method for ring oscillator simulation using the harmonic balance method recognizes that the manner in which the ring oscillator circuit is converted to a forced circuit plays a critical role in convergence. A more effective way of converting the ring oscillator circuit to a forced circuit is accomplished with the help of multiple probes. Although multiple probes are applied in the circuit, the initial guess still remains the same as that of the single-probe method by taking advantage of the ring oscillator phase relationships.

#### 5.5.1 *Application of Multiple Probes*

To show how the divergence in the bottom-level probe forced circuit occurs, the Newton iterative process for the fundamental and 2<sup>nd</sup> harmonic at different nodes for a single-ended 9-stage ring oscillator (Circuit 1 in Table 5.2) is shown in Figure 5.9. The Newton iterative process starts from some initial value. At the first iteration the fundamental voltages at some nodes go to a large number while all the 2<sup>nd</sup> harmonics are still reasonable. However, at the second iteration the 2<sup>nd</sup> harmonics diverge quickly due to the divergence of the fundamental circuit waveform at the previous iteration. The same trend can be seen with other higher order harmonics.

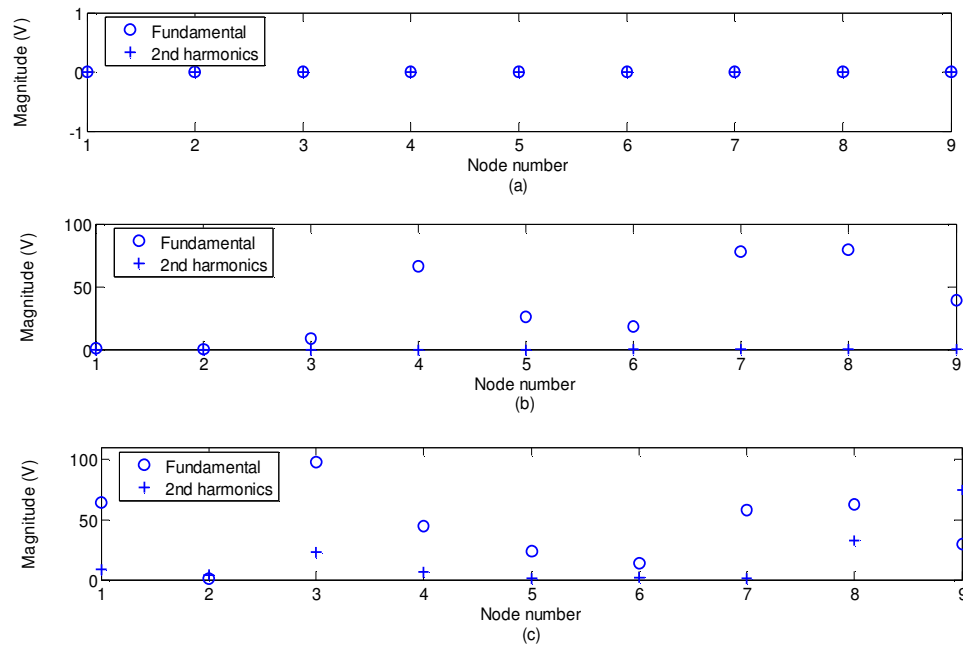
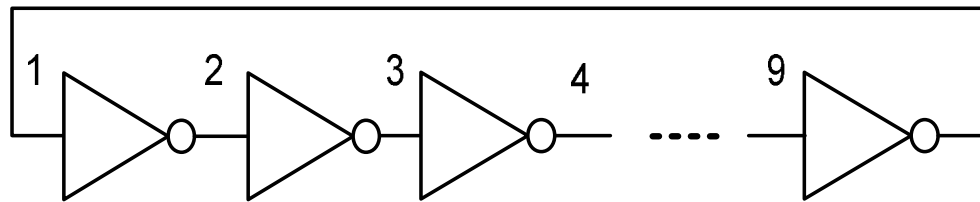


Figure 5.9: Newton iterative process for the fundamental and 2<sup>nd</sup> harmonic at different nodes and different iterations. (a) initial guess, (b) iteration #1, (c) iteration #2.

Based on above observation, a new way of forcing the ring oscillator circuit has been developed using multiple probes. A voltage probe is applied at the input of each delay cell as shown in Fig. 5.10. By doing so, the fundamental voltage waveform at all the important nodes in ring oscillator circuits are forced, which helps in constraining the fundamental waveform and thus avoiding convergence

problems as demonstrated in Fig. 5.9. For differential ring oscillators, voltage probes are added to the circuit at the oscillation frequency differentially.

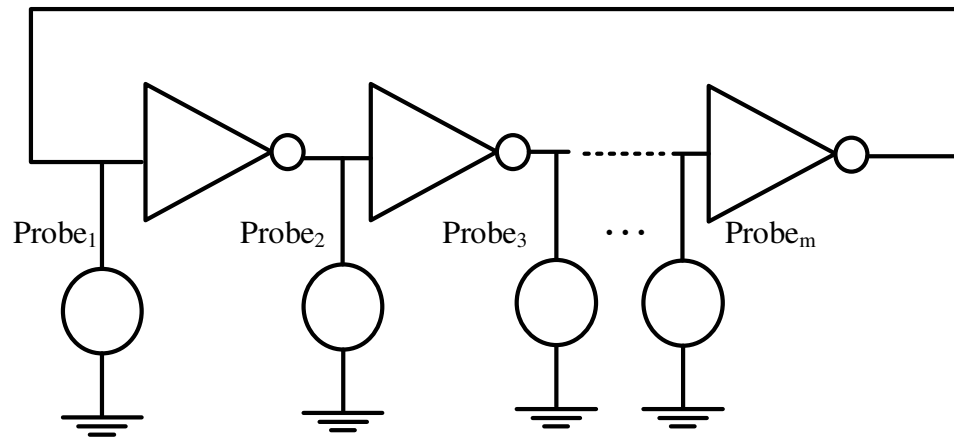


Figure 5.10: Ring oscillator simulation using multiple voltage probes.

For most ring oscillator circuits, there is no need to apply as many voltage probes as the number of stages. Simulations that fail with a single probe can converge readily with the application of two or more voltage probes. However, some ring oscillator circuits do require  $m$  (the number of the stages in the ring oscillator) voltage probes for reliable convergence. For a certain ring oscillator structure it is difficult to determine the minimum number of voltage probes or where these probes should be placed. For this reason voltage probes are generally applied at the input of each stage. Although a larger number of probes are used, the increase in the computational effort at each bottom level iteration is small as shown later in Section 5.5.4.

### 5.5.2 Initial Guesses for Multiple Probes

Since each voltage probe requires its own initial guess, multiple probes require multiple guesses, which can be an impractical task for most circuits. However, ring oscillators have a periodic structure and when all delay cells are identical the waveforms at the different nodes differ only in phase by an angle given in Eq. (5.2). If one voltage probe is chosen as a reference, the initial guess for all other voltage probes can be obtained by a phase shift using Eq. (5.3). Even when there are mismatches between cells, Eq. (5.3) still serves as a good approximation. For differential ring oscillators, the phase relationship in Eq. (5.3) holds for differential waveforms.

### 5.5.3 Solution by Newton's Method

The multiple-probe method is also implemented by a two-level Newton procedure. The bottom level of the two-level method solves the harmonic balance equations of the multiple-probe forced circuit. The sine part of one probe voltage is set to zero to fix the phase and this probe voltage is also used as a reference for the initial guess of the other probes. The bottom-level equation can be expressed as

$$\begin{bmatrix} J & e_1^c(1) & e_1^s(1) & \cdots & e_m^c(1) & e_m^s(1) \\ e_1^c(1) & 0 & 0 & \cdots & 0 & 0 \\ e_1^s(1) & 0 & 0 & \cdots & 0 & 0 \\ \vdots & \vdots & \vdots & \ddots & \vdots & \vdots \\ e_m^c(1) & 0 & 0 & \cdots & 0 & 0 \\ e_m^s(1) & 0 & 0 & \cdots & 0 & 0 \end{bmatrix} \begin{bmatrix} X^{(j+1)} \\ I_{1,probe}^{c(j+1)} \\ I_{1,probe}^{s(j+1)} \\ \vdots \\ I_{m,probe}^{c(j+1)} \\ I_{m,probe}^{s(j+1)} \end{bmatrix} = \begin{bmatrix} RhsF \\ V_{1,probe}^c \\ 0 \\ \vdots \\ V_{m,probe}^c \\ V_{m,probe}^s \end{bmatrix} \quad (5.14)$$

where  $J$  is the circuit Jacobian matrix.  $e_m^c(1)$  ( $e_m^s(1)$ ) is the unit vector that selects the cosine (sine) part of the first harmonic of the  $m$ th cell input node to which the

probe is attached.  $I_{m,probe}^c$  ( $I_{m,probe}^s$ ) is the cosine (sine) part of the corresponding probe current.

The top level solves the probe equations (Eq. (5.15)) where the probe voltages and frequency are updated until convergence is reached when the currents through all the voltage probes go to zero.

$$\begin{aligned}
 I_{1,probe}^c(V_{1,probe}^c, \dots, V_{m,probe}^c, V_{m,probe}^s, \omega) &= 0 \\
 I_{1,probe}^s(V_{1,probe}^c, \dots, V_{m,probe}^c, V_{m,probe}^s, \omega) &= 0 \\
 &\vdots \\
 I_{m,probe}^c(V_{1,probe}^c, \dots, V_{m,probe}^c, V_{m,probe}^s, \omega) &= 0 \\
 I_{m,probe}^s(V_{1,probe}^c, \dots, V_{m,probe}^c, V_{m,probe}^s, \omega) &= 0
 \end{aligned} \tag{5.15}$$

The Jacobian for this set of equations is:

$$J_{probe} = \begin{bmatrix} \frac{\partial I_{1,probe}^c}{\partial \omega} & \frac{\partial I_{1,probe}^c}{\partial V_{1,probe}^c} & \dots & \frac{\partial I_{1,probe}^c}{\partial V_{m,probe}^c} & \frac{\partial I_{1,probe}^c}{\partial V_{m,probe}^s} \\ \frac{\partial I_{1,probe}^s}{\partial \omega} & \frac{\partial I_{1,probe}^s}{\partial V_{1,probe}^c} & \dots & \frac{\partial I_{1,probe}^s}{\partial V_{m,probe}^c} & \frac{\partial I_{1,probe}^s}{\partial V_{m,probe}^s} \\ \vdots & \vdots & \ddots & \vdots & \vdots \\ \frac{\partial I_{m,probe}^c}{\partial \omega} & \frac{\partial I_{m,probe}^c}{\partial V_{1,probe}^c} & \dots & \frac{\partial I_{m,probe}^c}{\partial V_{m,probe}^c} & \frac{\partial I_{m,probe}^c}{\partial V_{m,probe}^s} \\ \frac{\partial I_{m,probe}^s}{\partial \omega} & \frac{\partial I_{m,probe}^s}{\partial V_{1,probe}^c} & \dots & \frac{\partial I_{m,probe}^s}{\partial V_{m,probe}^c} & \frac{\partial I_{m,probe}^s}{\partial V_{m,probe}^s} \end{bmatrix} \tag{5.16}$$

This  $2m \times 2m$  Jacobian can be obtained by a simple computation using information from the bottom-level solution.

The frequency-domain nonlinear equations for the circuit-probe combination,  $G$ , can be expressed as:

$$G(X_A, \omega) = 0 \tag{5.17}$$

where  $x_A$  is the vector of circuit unknowns and the probe currents. The sensitivity with respect to  $\omega$  and each probe voltage can then be computed as:

$$\begin{aligned}
 \frac{\partial G}{\partial X_A} \frac{\partial X_A}{\partial \omega} &= -\frac{\partial G}{\partial \omega} \\
 \frac{\partial G}{\partial X_A} \frac{\partial X_A}{\partial V_{1,probe}^c} &= -\frac{\partial G}{\partial V_{1,probe}^c} \\
 &\vdots \\
 \frac{\partial G}{\partial X_A} \frac{\partial X_A}{\partial V_{m,probe}^c} &= -\frac{\partial G}{\partial V_{m,probe}^c} \\
 \frac{\partial G}{\partial X_A} \frac{\partial X_A}{\partial V_{m,probe}^s} &= -\frac{\partial G}{\partial V_{m,probe}^s}
 \end{aligned} \tag{5.18}$$

where  $\frac{\partial G}{\partial X_A}$  is the augmented Jacobian in Eq. (5.14). Since the augmented Jacobian matrix is already factored in the bottom level, only forward and backward substitutions are needed to solve Eq. (5.18). All entries of the  $2m \times 2m$  Jacobian matrix in Eq. (5.16) can be easily extracted from the solution of Eq. (5.18).

#### 5.5.4 Computational Effort Analysis

Since multiple probes are applied to the circuit, there is a need to analyze the computational effort. The total computational effort for the two-level method is dominated by the bottom level due to two reasons. First, the bottom-level circuit unknowns are much larger in number than the top-level probe unknowns. Second, in the general case, the number of bottom-level iterations is several times larger than the number of top-level iterations.

From Eq. (5.14) we can see that although multiple voltage probes have been used, the bottom level matrix size increases only by  $2(m-1)$  (where  $m$  is the

number of probes) which is negligible compared to the bottom-level matrix size. Therefore, the increase in computational effort for each bottom-level iteration is minimal. The multiple-probe method is almost no more expensive than the traditional single-probe method for each bottom-level iteration.

The single-delay cell method and the multiple-probe method have been tested on a wide variety of single-ended and differential ring oscillators to show their performance. The simulation results are summarized in Chapter 7.

## **5.6 Summary**

In this chapter two novel ways of simulating ring oscillators with the harmonic balance method are described. Both of the approaches exploit the phase relationships of a ring oscillator. Details of the numerical formulation and implementation are given. The proposed single-delay cell method assumes that all the oscillator cells are identical and cannot be used when large mismatches between cells need to be accounted for. The multiple-probe method is a more general method which can be used instead.

## 6. FREQUENCY DOMAIN SIMULATION OF RELAXATION OSCILLATORS

The operation of relaxation oscillators is based on charge and discharge of capacitors with a constant current between two threshold levels. The circuit waveforms have very sharp transitions. Therefore harmonic truncation produces large aliasing errors which makes the standard harmonic balance method not suitable for the simulation of relaxation oscillators.

### 6.1 Relaxation Oscillator Frequency Spectrum

The time-domain waveform as well as the frequency domain spectrum for a simple CMOS relaxation oscillator (Fig. 6.1) are shown in Fig. 6.2. From the figure we can see that one of the circuit waveforms has a very sharp transition and the signal power decreases very slowly with an increase in the number of harmonics. In theory, for waveforms with sharp transitions the Fourier coefficients are proportional to  $\frac{1}{n}$ , where  $n$  is the number of harmonics. So harmonic truncation will introduce significant aliasing error.

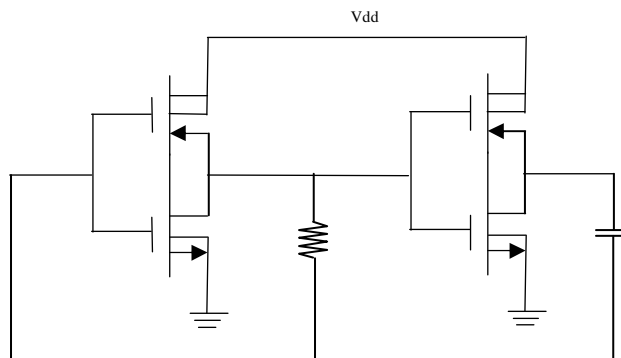


Figure 6.1: Schematic of a CMOS relaxation oscillator.

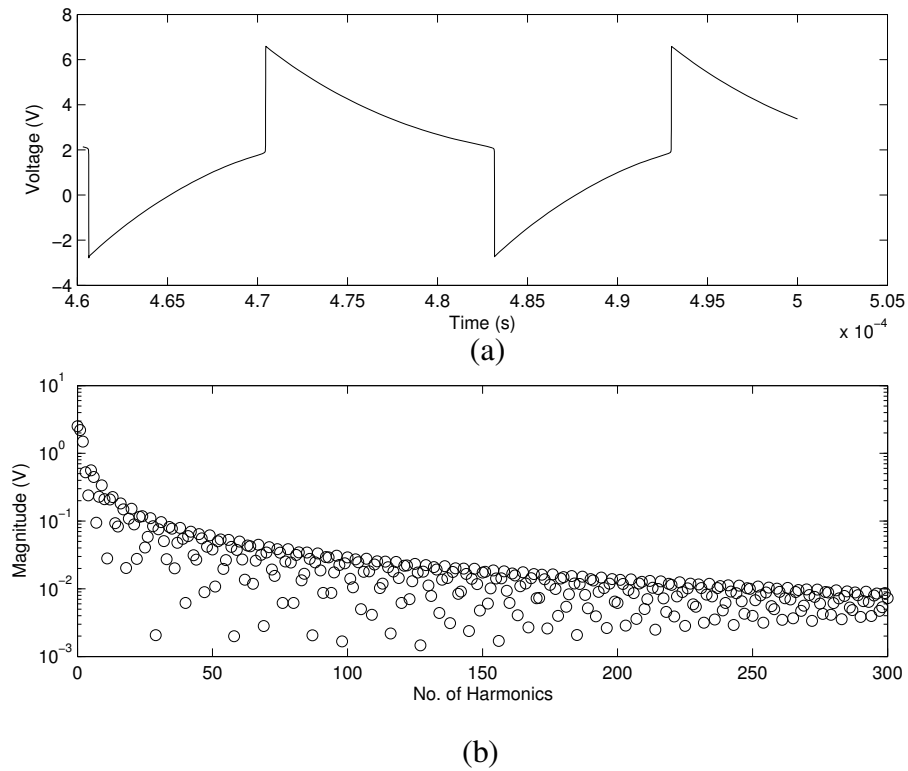


Figure 6.2: Time-domain waveform and frequency spectrum for a relaxation oscillator.

## 6.2 Aliasing Error for Relaxation Oscillator Simulation

The relaxation oscillator in Fig. 6.1 is simulated with the harmonic balance method to show the influence of the aliasing error. The oscillation frequency solution from the harmonic balance method using a different number of harmonics is shown in Fig. 6.3. From the figure we can see that with an increased number of harmonics in the simulation, the solution gets closer to the actual solution. However, even with more than 100 harmonics, it is still off by a factor of 2. The frequency spectrum of the circuit waveform is shown in Fig. 6.4, along with the result from a transient analysis. The discrepancy between the results from

the harmonic balance method and the transient analysis shows the extent of aliasing errors. Fig. 6.5 gives a clear picture how this aliasing error influences the time-domain circuit waveform solution.

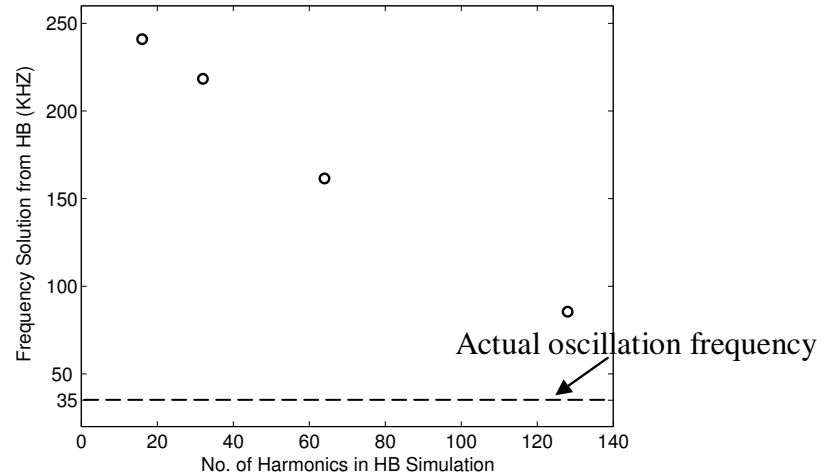


Figure 6.3: Oscillation frequency solution from the harmonic balance method using a different number of harmonics.

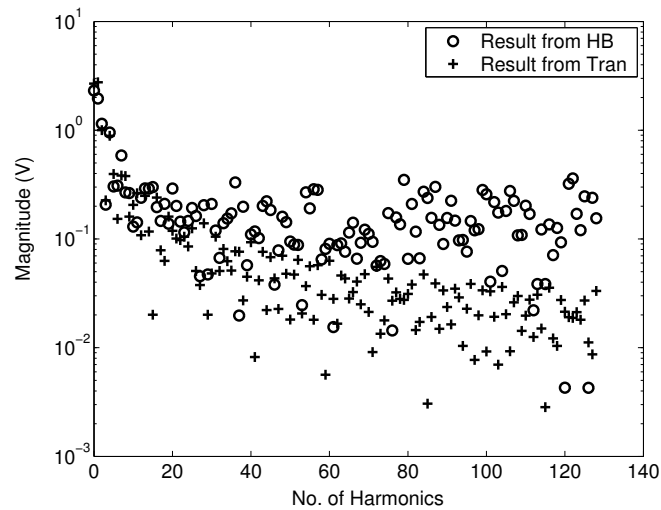


Figure 6.4: Frequency spectrum from transient analysis and harmonic balance method with 128 harmonics.

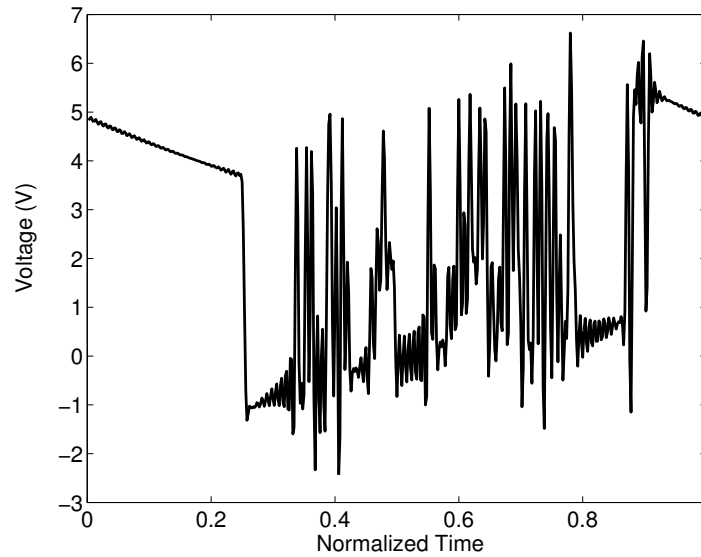


Figure 6.5: Time-domain waveform from the harmonic balance method with 128 harmonics.

One observation is that to faithfully represent the circuit waveforms and effectively control the aliasing error, harmonic truncation needs to take into consideration harmonics whose magnitude is greater than about one-thousandth that of the fundamental. For relaxation oscillators this means that more than a thousand harmonics need to be chosen for moderate accuracy. So the standard harmonic balance method is not suitable for simulation of relaxation oscillators.

## 7. EXAMPLES AND RESULTS

### 7.1 Frequency-Domain Simulation of High-Q Oscillators

The new homotopy algorithms developed in Chapter 4 are used to solve different high-Q oscillators where the conventional two-level method fails. The results from the homotopy-harmonic balance combined method are verified with the results from long and expensive transient simulations. The developed method is also used to simulate moderate Q oscillators and then the computational performance of the two-level method and the homotopy method is compared.

#### 7.1.1 High-Q Oscillator Examples

The first example is the Pierce oscillator as shown in Fig. 4.2. The voltage probe is attached at the high impedance collector node of the BJT. The frequency from a pole-zero analysis is used as the initial frequency and a 1mV initial value is used for the probe voltage. For this example, the whole process takes 9 homotopy steps for  $\lambda_1$ . The total number of iterations (Jacobian evaluations) for Algorithm 1 and Algorithm 2 is 942 and 304, respectively. The oscillation frequency is found to be 9.998422MHz. The solution tracks for the probe voltage and the corresponding frequency using Algorithm 1 and Algorithm 2 are the same as shown in Fig. 7.1. From the figure we can see that both the frequency and the probe voltage solution tracks rapidly progress towards the solution. From  $\lambda = 0$  to about  $\lambda = 0.2$ , the frequency changes quickly, and the tracking takes much fewer steps compared with that of Fig. 4.4. This is a clear benefit obtained by decoupling the frequency and the probe voltage.

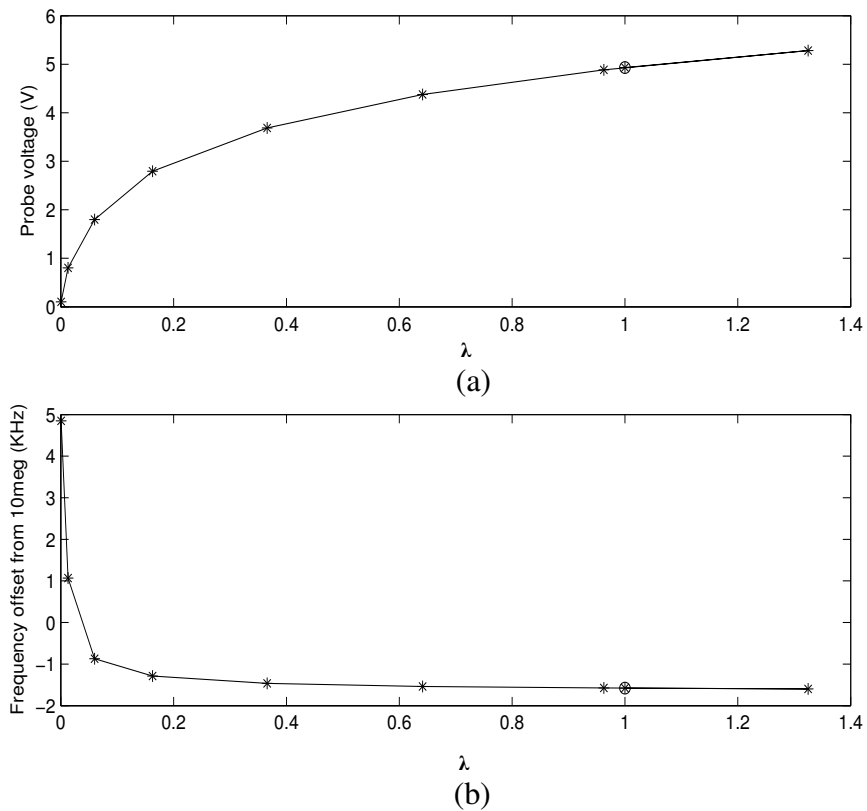


Figure 7.1: Solution traces for the Pierce oscillator using the new algorithm. (a) Probe voltage as a function of  $\lambda$ . (b) Oscillation frequency as a function of  $\lambda$ .

The detailed information on the number of steps at Step 1 (Fig. 4.5 and Fig. 4.7) for each  $\lambda_1$  using Algorithm 1 and Algorithm 2, respectively, is summarized in Table 7.1. Algorithm 2 provides a speed-up over Algorithm 1 since Newton's method instead of the homotopy method is used to solve for the frequency. This illustrates that Algorithm 2 is efficient and it is used for all subsequent examples in this section.

Table 7.1: Newton iteration information for each  $\lambda_1$  step for the Pierce oscillator using Algorithm 1 and Algorithm 2.  $\Delta\lambda_1$  is the  $\lambda_1$  increment from the previous  $\lambda_1$  point.

$\lambda_1$ step	$\Delta\lambda_1$	Algorithm 1	Algorithm 2
		# $\lambda_2$ steps	# Newton steps
1	0.0006	22	7
2	0.012	31	8
3	0.0047	21	7
4	0.10	18	6
5	0.20	16	6
6	0.27	14	5
7	0.32	12	6
8	0.36	13	4
9	-0.32	9	3

To verify the accuracy of the homotopy method, a long and expensive transient analysis with tight tolerances is performed for the Pierce oscillator. The CPU time is about 1000 times that of the homotopy based harmonic balance method. The steady-state output voltage in both the time and frequency domains is shown in Fig. 7.2 along with the results from a transient analysis. From the plot we can see that the results from the homotopy based harmonic balance analysis and transient analysis are in good agreement.

To show the robustness of this method several high-Q oscillators were simulated. In the following examples, the two-level method failed because an initial guess for the probe voltage could not be determined whereas the new homotopy based algorithm converged. Table 7.2 shows the starting frequency  $f_o$ ,

the ratio of the final frequency  $f$  to  $f_o$ , the number of homotopy steps, the total number of iterations, and the CPU times on a SUN Ultra10 workstation. Fig. 7.3 and Fig. 7.4 show the schematic and tracking curves for the Pierce2 oscillator.

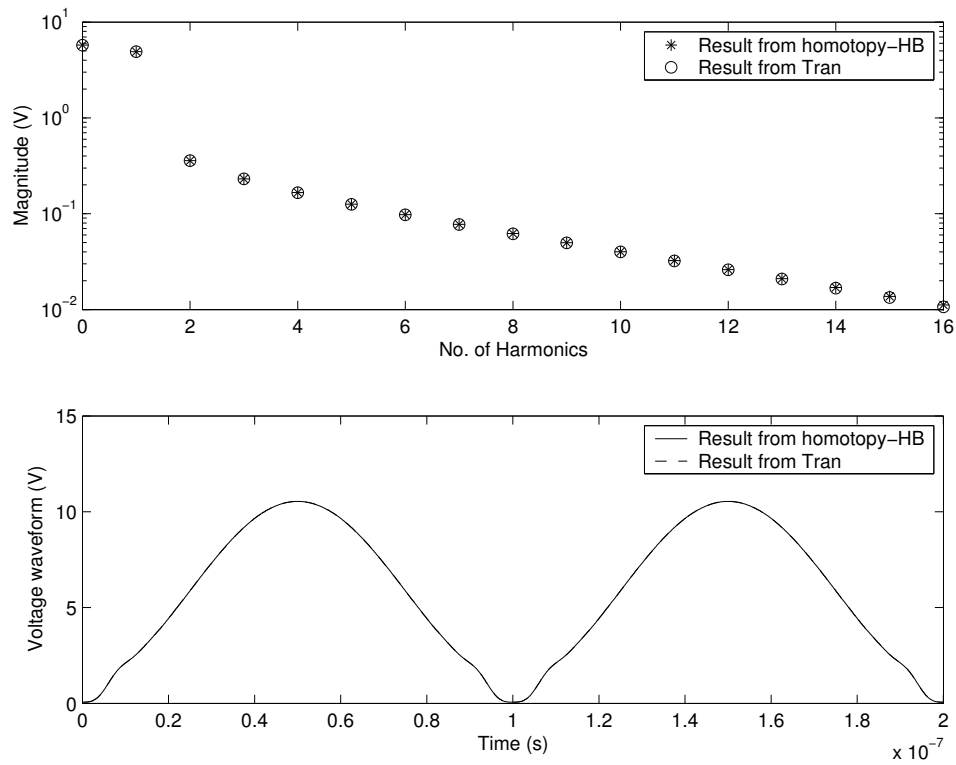


Figure 7.2: Results from transient and homotopy based harmonic balance simulations of the Pierce oscillator.

Table 7.2: Results for various high-Q oscillators.

Circuit	Q	$f_o$ (MHz)	$f/f_o$	# Steps	#Iter	CPU time (sec)
Colpitts	$1.00 \times 10^3$	1.5915	0.99987	11	208	17.5
TNT	$1.02 \times 10^3$	11.795	0.84738	15	492	26.3
Pierce (BJT)	$1.07 \times 10^4$	4.0811	0.97036	10	241	13.2
Pierce1 (MOS)	$3.69 \times 10^4$	7.9992	0.99907	5	98	8.2
Clapp	$1.14 \times 10^5$	20.124	0.99998	12	243	19.2
Pierce2 (MOS)	$2.82 \times 10^5$	1.1256	0.99995	26	403	141

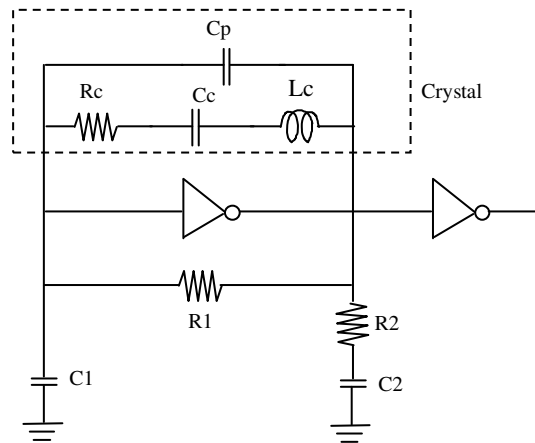


Figure 7.3: Circuit schematic of the Pierce oscillator with MOS inverter.  $R1=1\text{M}\Omega$ ,  $R2=2.7\text{K}\Omega$ ,  $C1=55\text{pF}$ ,  $C2=60\text{pF}$ ,  $Cp=25\text{pF}$ ,  $Cc=10\text{fF}$ ,  $Rc=60\Omega$ ,  $Lc=2\text{H}$ .

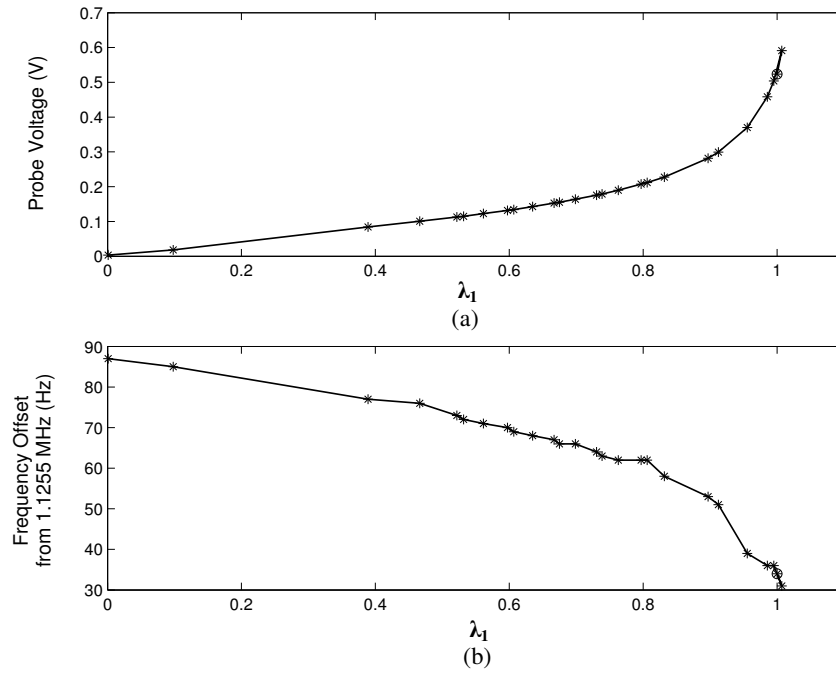


Figure 7.4: Solution traces for the high Q Pierce oscillator (Pierce2) using the new algorithm. (a) Probe voltage as a function of  $\lambda_1$ . (b) Oscillation frequency as a function of  $\lambda_1$ .

Oscillator simulation with numerical models is even more difficult than the analytical models as discussed in [23]. The new algorithm is also robust in this case. Algorithm 2 has been implemented in the coupled device and circuit simulator, CODECS [45]. For the Pierce 1 oscillator in Table 7.2. The tracking takes 7  $\lambda_1$  step with 298 total iterations. The solution track is shown in Fig. 7.5.

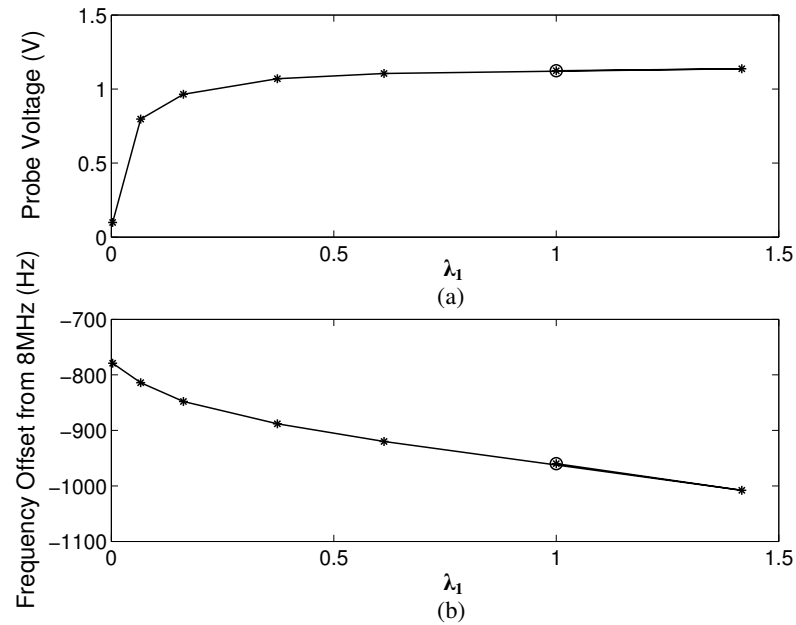


Figure 7.5: Solution traces for the Pierce oscillator (Pierce1) with numerical models using the new algorithm. (a) Probe voltage as a function of  $\lambda_1$ . (b) Oscillation frequency as a function of  $\lambda_1$ .

### 7.1.2 Moderate-Q Oscillator Examples

The proposed homotopy method is not limited to high-Q oscillators only. Oscillators with moderate Q have also been tested [41]. The results are summarized in Table 7.3. The total number of iterations required for the two-level method (for the initial guess and for solving Eqs. (3.8) and (3.9)) is smaller than that for the homotopy method when the two-level method converges. In these situations, the homotopy method is less than 10 times expensive in the worst case, and for most circuits it is only 2-4 times slower. However, the two-level method does not converge for oscillator circuits with numerical models whereas the homotopy method does (Table 7.3). These examples illustrate that the new homotopy-based algorithm is robust for a wide range of circuits and models.

Table 7.3: Comparison of the two-level method and homotopy method for moderate-Q oscillator circuits. # indicates circuits with numerical models, and × denotes circuits that fail to converge.

Circuit	# Iterations			CPU time (sec)	
	Two-level		Homotopy	Two-level	Homotopy
	Initial guess	Eqs. (5), (6)			
Colpitts (BJT)	44	19	197	1.6	5.2
Colpitts (MOS)	52	21	208	2.1	6.3
TNT	113	57	310	12.6	23.4
Wien	64	29	274	6.1	14.5
Sony	56	32	170	5.6	12.1
Phase shift	40	17	307	23.9	127.2
Source coupled	58	16	358	12.8	60.1
Emitter coupled Colpitts	43	16	256	7.5	36.7
Cross coupled	45	24	398	3.1	20.8
Colpitts(MOS) #	×	×	172	×	854.4
Sony #	×	×	593	×	581.2

## 7.2 Frequency-Domain Simulation of Highly Nonlinear Ring Oscillators

In this section, the two new proposed methods, the single-delay cell method and the multiple-probe method are evaluated on a variety of single-ended and

differential ring oscillator circuits. The convergence performance as well as the accuracy of the two methods is demonstrated. The single-delay cell method provides a significant speed-up over the conventional approach as shown. The multiple-probe method is efficient and converges robustly for a wide variety of ring oscillator circuits with non-identical delay cells.

### ***7.2.1 Convergence Performance and Accuracy***

To show the robustness of the proposed single-delay cell and multiple-probe methods, circuits from Table 5.2 have been simulated. The results are summarized in Table 7.4. From the results we can see that the two proposed methods converge robustly for those circuits where the traditional approach fails. The two approaches show nearly the same convergence properties and the convergence is not sensitive to the initial probe voltage and the oscillation frequency guess.

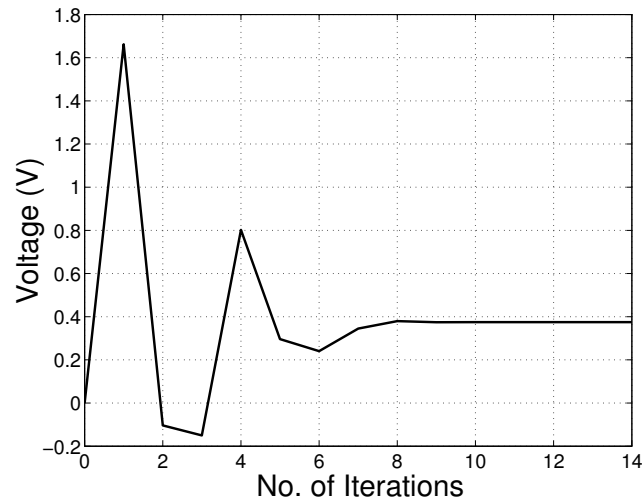
The frequency initial guess is estimated from the time-delay of the delay cells, which can be obtained from the step-response of the delay cell. The probe voltage initial guess is simply chosen based on the power supply voltage. For full-swing delay cells, such as those in Circuit 1, this is a good initial guess since the output swing is constrained by the power supply. However, for partial-swing delay cells (Circuits 2, 3, 4) the circuit structure also plays a role, and the probe voltage guess depends on the circuit. The new single-delay cell and multiple probe methods converge robustly for ring oscillator circuits with partial-swing delay cells even with the power supply voltage used as the initial probe voltage. This characteristic makes the application of the harmonic balance method to ring oscillator simulation even easier since the only initial guess that needs to be specified is the oscillation frequency. Furthermore, as shown in the Table 7.4 this can be off by more than 50%.

From Table 7.4 we can see that the convergence of the ring oscillator top-level probe equation is not sensitive to the initial guess whenever the bottom-level iteration converges. This is consistent with the low Q nature of ring oscillator circuits. However, if the conventional method [7] is used and the initial guess is too far from the real solution, the bottom-level equations fail to converge before the frequency and probe voltage can even be updated at the top level.

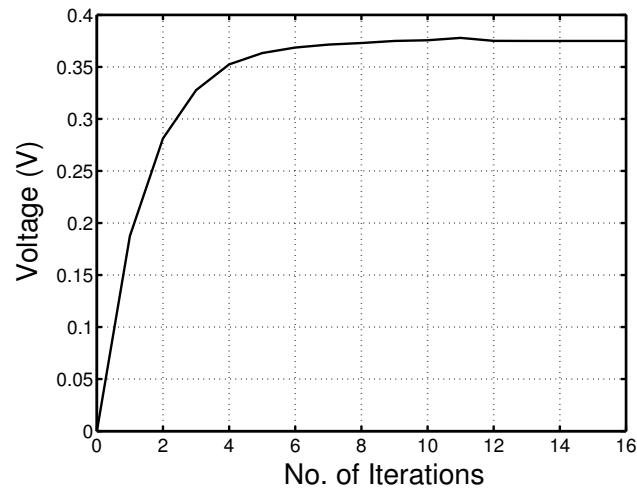
Table 7.4: Convergence sensitivity to initial guess for different ring oscillator circuits using the new single-delay cell and multiple-probe methods.

Delay cell	Circuit 1	Circuit 2	Circuit 3	Circuit 4
$ \Delta f /f_{osc}$	>50%	>50%	>50%	>50%
$ \Delta V_{probe} /V_{osc}$	19.5%	33.5%	46.7%	24.5%

To show the convergence process of the new methods, the same circuit waveform (as that in Fig. 5.2) during the Newton iterative process using the single-delay cell and multiple-probe methods is shown in Fig. 7.6. It can be seen that both methods constrain the circuit waveform while requiring no damping or any thresholds. Also the convergence is achieved in only a few iterations.



(a)



(b)

Figure 7.6: Circuit waveform during the Newton iterative process. (a) Single-delay cell method. (b) Multiple-probe method.

The steady-state output voltage in both the time and frequency domains for Circuit 1 is shown in Fig. 7.7 along with the results from a transient analysis to

show the accuracy of the new methods. From the plots we can see that the results from the single-delay cell and multiple-probe harmonic balance methods are in good agreement with those from the transient analysis.

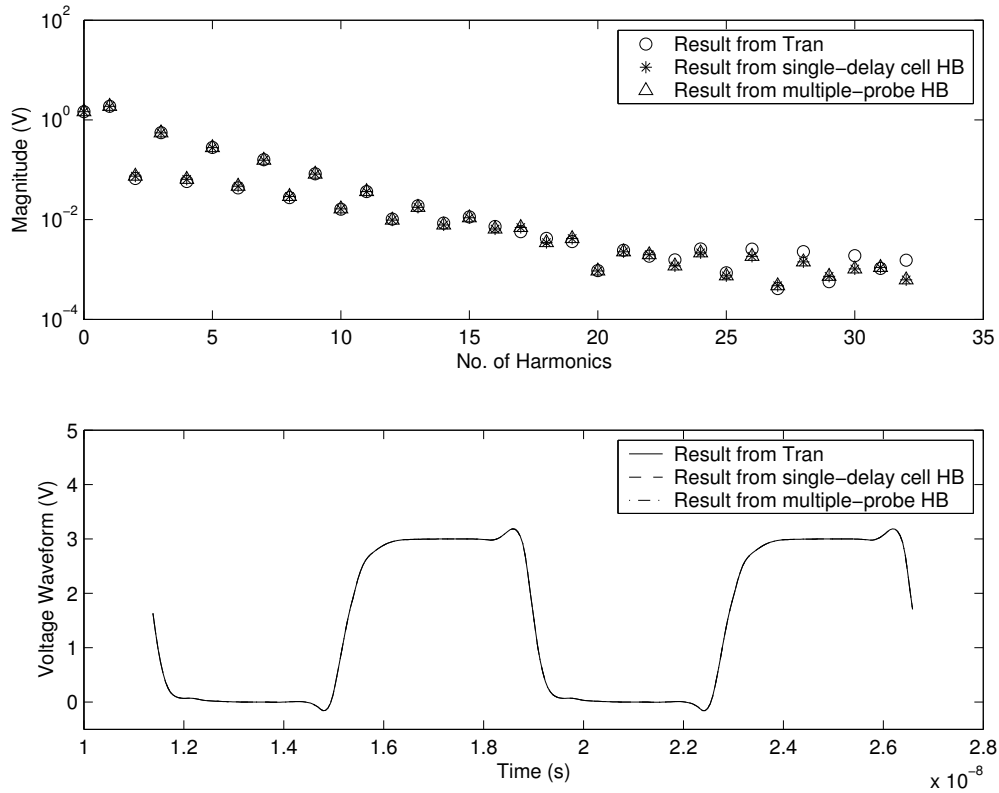


Figure 7.7: Results from transient, single-delay cell harmonic balance, and multiple-probe harmonic balance simulations of a 9-stage ring oscillator.

### 7.2.2 Computational Performance of the Single-delay Cell Method

The new single-delay cell method is very efficient for ring oscillator simulation. Several single-ended and differential ring oscillators have been simulated using the conventional approach and the new single-delay cell

approach. The inverters are implemented by the current-starved delay cell (Fig. 5.1(b)) and the cross-coupled load delay cell (Fig. 5.1(d)), respectively. From the simulation results in Table 7.5 we can see that the single-delay cell method provides a significant speed-up in simulations even for a 3 stage differential ring oscillator. The number of iterations for the single-delay-cell method is also less than the complete oscillator simulation due to a smaller number of nonlinear devices.

Table 7.5: Comparison of the conventional approach with the new single-delay cell approach for ring oscillators.

Circuit	Method	#Unknowns	Matrix size	# Iterations	Memory (M)	CPU time(min)
1	Conventional	19	933×933	201	20.7	20.25
	Delay cell	7	345×345	97	8.84	0.70
2	Conventional	69	1727×1727	355	18.2	39.63
	Delay cell	31	777×777	131	11.3	2.55

Circuit 1: 15-stage single-ended ring oscillator with current starved delay cell.

Circuit 2: 3-stage differential ring oscillator with cross-coupled load delay cell.

One key benefit of the single-delay cell method is that ring oscillators with a different number of stages can be simply simulated by using the single-delay cell equivalent circuit with the value of the phase delay  $\theta$  adjusted according to Eq. (5.2). The simulation results are presented in Tables 7.6 and 7.7 for a single-ended ring oscillator and a differential ring oscillator, respectively. The current-starved delay cell (Fig. 5.1(b)) and the Maneatis delay cell [42] (Fig. 7.9(a)) are used.

From the tables, we see that the more the number of stages, the higher the nonlinearity, and therefore, the more the CPU time required for convergence. However, for the single-delay cell method, the CPU time only increases by a factor of 2-3 whereas for the conventional method, the simulation time increases by a factor of 40 for the 21-stage single-ended ring oscillator and the convergence is very sensitive to the initial guess. For differential ring oscillators with more than 3 stages the conventional method failed to reach convergence. The slight increase in the CPU time for the single-delay cell method with an increased number of stages, is due to the circuit operation becoming more and more nonlinear.

Table 7.6: Comparison of simulation results for single-ended ring oscillators with different number of stages.

#Stages		5	7	11	15	17	19	21
CPU time (min)	Single-delay Cell Method	0.15	0.18	0.20	0.23	0.25	0.28	0.42
	Conventional Method	0.62	2.60	4.12	6.55	10.92	17.88	25.35
Memory (M)	Single-delay Cell Method	7.2	7.2	7.2	7.2	7.2	7.2	7.2
	Conventional Method	8.9	9.7	11.2	12.6	13.2	14.1	15.3

Table 7.7: Comparison of simulation results for differential ring oscillators with different number of stages. × denotes no convergence under exact initial guess for the oscillation frequency and probe voltage.

#Stages		3	5	7	9
CPU time (min)	Single-delay Cell Method	2.31	3.22	4.00	4.85
	Conventional Method	34.63	×	×	×
Memory (M)	Single-delay Cell Method	10.9	10.9	10.9	10.9
	Conventional Method	17.2	23.5	35.7	53.4

The single delay cell method is also effective for differential ring oscillators with an even number of stages since the phase relationship for each delay cell still holds. A 4-stage differential ring oscillator (Fig. 7.8) is simulated with three kinds of delay cells: Maneatis delay cell [42], Lee/Kim delay cell [43] and current-controlled delay cell [44] (Fig. 7.9). All circuits converge robustly and the performance is summarized in Table. 7.8. There is also a good agreement between the results from the harmonic balance method and transient analysis as shown in Figure 7.8 for the current-controlled delay cell.

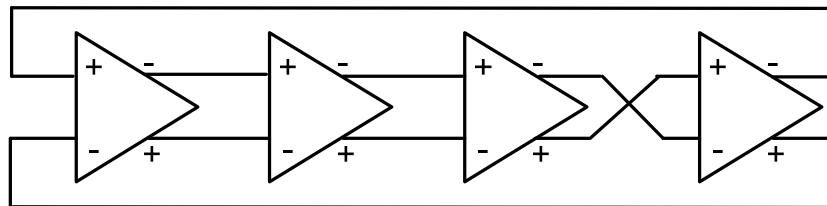


Figure 7.8: 4-stage differential ring oscillator.

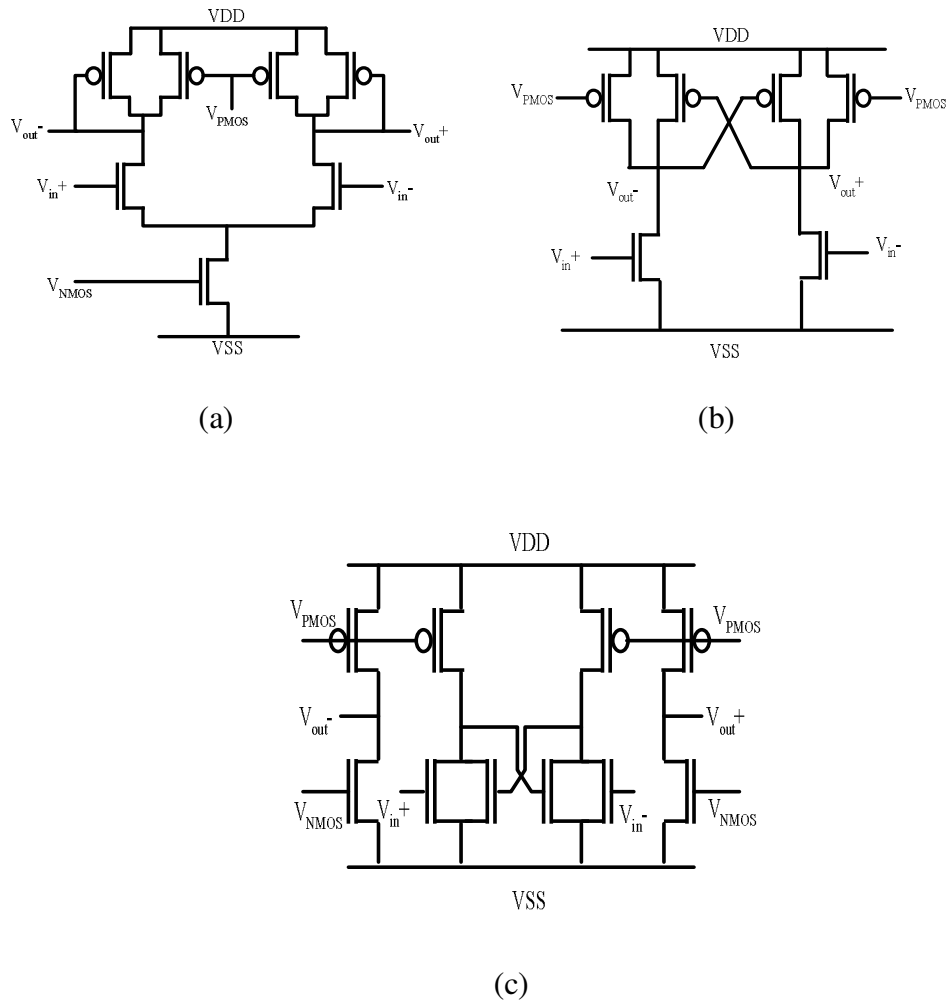


Figure 7.9: Ring oscillator delay cells. (a) Maneatis load delay cell. (b) Lee/Kim delay cell. (c) Current-controlled delay cell.

Table 7.8: Simulation performance comparison for the four-stage differential ring oscillators with different delay cells using the single-delay cell approach.

Delay cells (Fig. 7.9)	#Unknowns	Matrix size	# Iterations	CPU time(min)
(a)	29	727×727	158	3.17
(b)	22	552×552	201	2.37
(c)	32	802×802	85	1.67

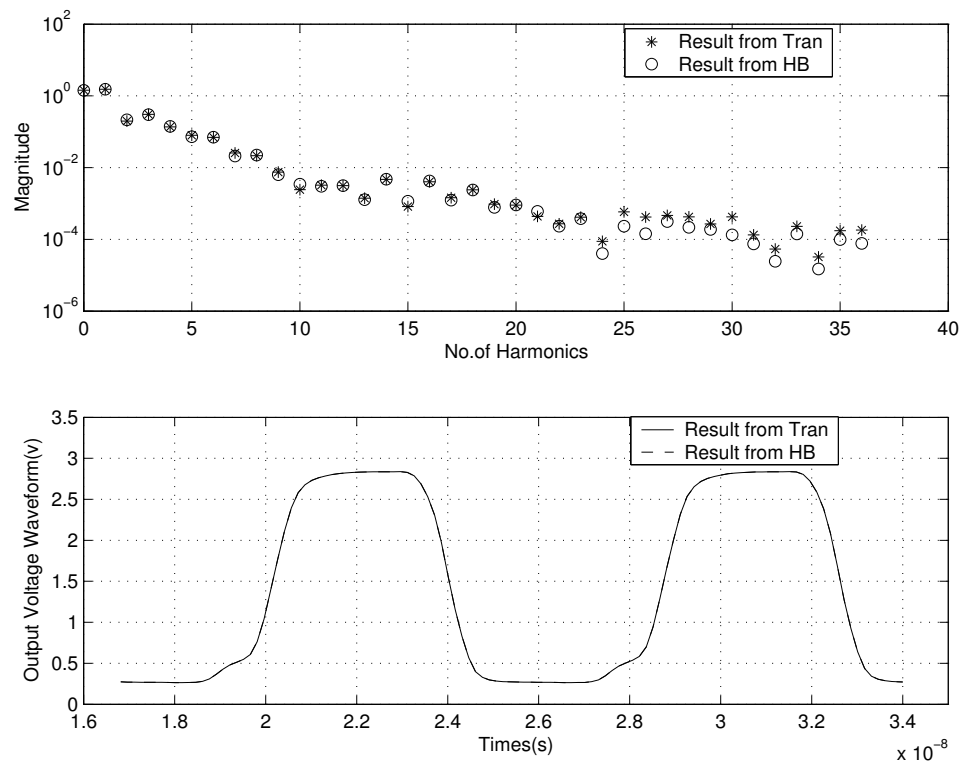


Figure 7.10: Simulation results for the 4-stage differential ring oscillator (current-controlled delay cell).

### 7.2.3 Computational Performance of the Multiple-probe Method

For ring oscillator circuits that converge with the conventional single probe method using a close initial guess, the multiple-probe method is more efficient even when more probes are applied in the circuit. The simulation results are shown in Table.7.9. In this case the matrix size and memory requirements for the two methods are similar. However, the multiple-probe method uses a more effective way to force the circuit, thereby requiring fewer iterations for convergence.

Table 7.9: Comparison of the multiple-probe method with the single-probe method for ring oscillator simulation.

Cir	# Stages	Delay cell	# Iterations (# Top level iterations)		CPU time Multiple-probe/Conventional Method
			Multiple-Probe Method	Conventional Method	
1	7	Fig. 5.1(a)	58 (6)	104 (5)	0.53
2	9	Fig. 5.1(b)	48 (4)	75 (4)	0.63
3	3	Fig. 5.1(d)	39 (5)	56 (5)	0.67
4	3	Fig. 7.9 (a)	64 (4)	90 (4)	0.71
5	4	Fig. 7.9 (b)	59 (6)	128 (7)	0.46

#### 7.2.4 Multiple-probe Method for Non-ideal Delay Cells

The single-delay cell method is very efficient as shown in Section 7.2.2. However, it cannot handle ring oscillators with non-identical delay cells. The multiple-probe method simulates the full ring oscillator circuit. No assumptions about identical delay cells are made, so it can be used to simulate non-identical delay cells. Next the effectiveness of the multiple-probe method for simulating ring oscillators with mismatched or non-identical delay cells is demonstrated. The results for several circuits are summarized in Table 7.10. The first circuit is connected to an output buffer and the second circuit was implemented using mismatches within the delay cells. For simplicity we assume the mismatches only exist between the input NMOSFET of each stage. From the table we can see that the proposed method converges robustly for these cases. The number of iterations with identical delay cell cases and mismatch/loading cases are quite similar.

Table 7.10: Comparison of ring oscillator simulation with identical delay cells and mismatched cells using the multiple-probe method.

Delay cell		Fig. 5.1 (a)		Fig. 7.9 (c)	
# Stages		5		4	
Oscillator circuit		Without output buffer	With output buffer	Identical cells	Mismatched cells
Oscillation frequency (MHz)		237.56	216.74	116.92	121.82
# Iter	Top level	8	7	5	5
	Bottom level	53	47	70	76

Though the initial guesses for multiple probes are based on the assumption of identical delay cells, the proposed method is able to handle ring oscillators with large mismatches in the delay cells. To demonstrate the robustness of the multiple-probe method, an extreme case is used. A nine-stage stepped buffer is connected as a ring oscillator configuration as shown in Fig. 7.11. The multiple-probe method converges and requires only 106 bottom level and 11 top level iterations while the single-probe method fails.

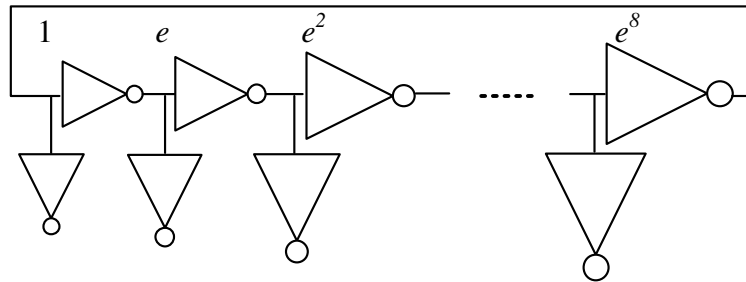


Figure 7.11: 9-stage stepped-buffer connected as a ring oscillator. Each stage is sized a factor of  $e$  larger than the previous stage.

### 7.2.5 Simulation of Ring Oscillators with Numerical Models

In this section, more accurate numerical models are used for ring oscillator simulation. The new algorithms for robust ring oscillator simulation are implemented in the coupled device and circuit simulator CODECS [24, 45]. A two-dimensional (2D) numerical MOSFET model with  $31 \times 19$  mesh points is used. While the single-probe method fails for these circuits with numerical models, the single-delay cell and multiple-probe methods deliver reliable convergence. The simulation results are the same for the two methods. Since circuit simulation with numerical models is very time-consuming, the single-delay cell method is preferred in these cases.

Table 7.11: Ring oscillator simulation results with 2D numerical MOSFET models.

Delay cells	Single-delay Cell Method			Multiple-probe Method		
	# Iterations (# Top level iterations)	CPU Time (min)	Memory (M)	# Iterations (# Top level iterations)	CPU Time (min)	Memory (M)
Fig. 5.1 (d)	270(5)	54.4	14.3	237 (5)	164.9	35.5
Fig. 7.9 (a)	98(5)	18.1	15.4	101 (5)	54.60	31.9
Fig. 7.9 (b)	136(5)	17.4	13.9	93 (4)	52.37	35.4
Fig. 7.9 (c)	121(4)	91.2	20.8	129 (6)	224.4	44.8

The influence of substrate noise on the output spectrum of the ring oscillator has also been studied with more accurate numerical models. The set-up for the simulation is as shown in Fig. 7.12. There are two tones in the circuit. One is the unknown oscillator frequency, the other is the substrate noise frequency. The problem thus becomes a mixer plus oscillator problem. In this particular example 52 harmonics were chosen by the box truncation method [2]. The simulation results with and without substrate noise are shown in Fig. 7.13. From the figure we can clearly see the effect of the substrate noise on the oscillator output spectrum.

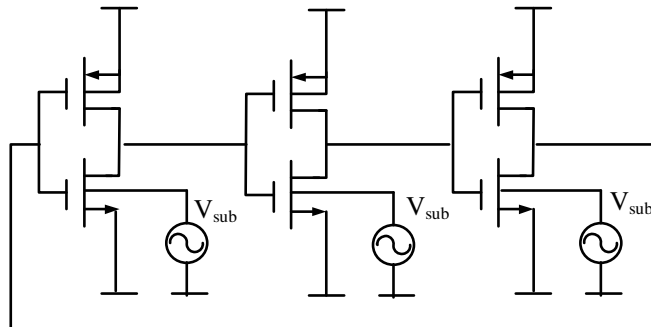


Figure 7.12: Ring oscillator simulation with substrate noise.  $f_{osc}=0.414\text{GHz}$ ,  $f_{sub}=0.8\text{GHz}$ ,  $V_{sub}=10\text{mV}$ .

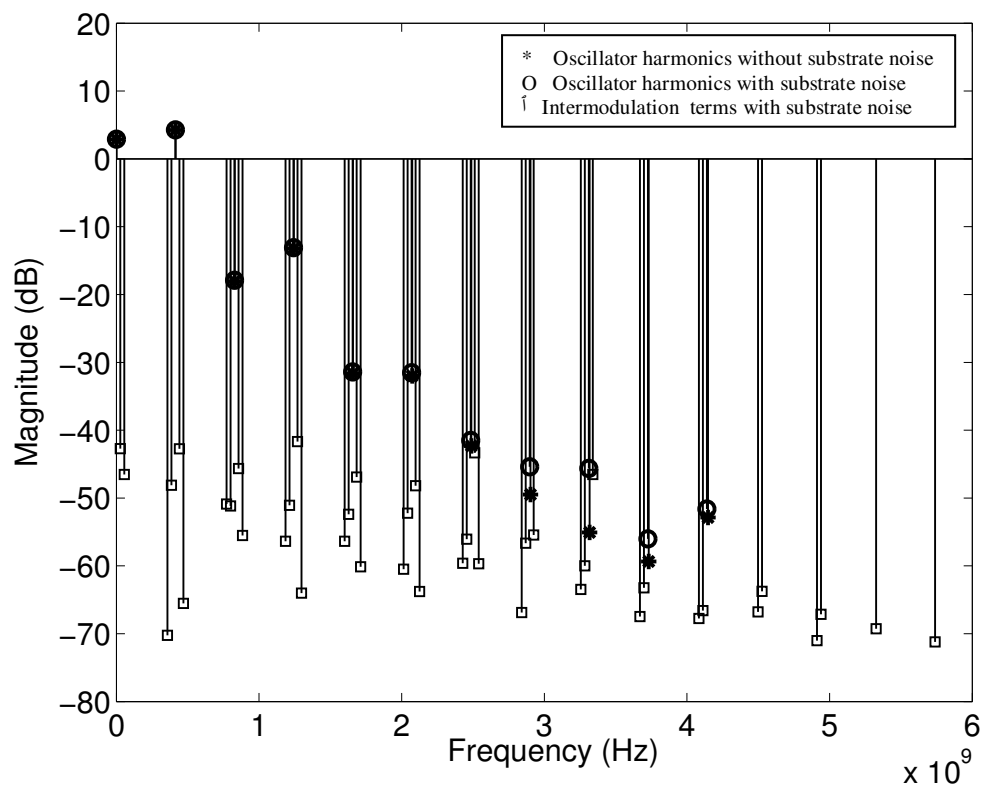


Figure 7.13: Simulation results for a 3-stage ring oscillator with substrate noise.

### 7.3 Summary

In this chapter, oscillator examples are used to show the performance of the proposed homotopy-based harmonic balance method, single-delay cell method and the multiple probe method.

The homotopy-based harmonic balance method is robust and efficient for the simulation of high-Q oscillators where the conventional two-level method failed. This method can also be used for the simulation of moderate Q oscillators with acceptable computational cost. While the two-level method fails for some oscillator circuits with numerical models, the homotopy-based harmonic balance method delivers reliable convergence.

The single-delay cell and multiple-probe methods solve the convergence problems in the simulation of ring oscillators. Both methods are robust and not sensitive to the initial guesses. The single-delay cell method provides a significant speed-up over the multiple-probe method.

## 8. CONCLUSIONS

### 8.1 Summary of Contributions

This work presents the first detailed study of frequency-domain simulation of oscillators using the harmonic balance method. The convergence problems encountered in different kinds of “hard-to-solve” oscillator circuits have been studied. New approaches for robust and efficient harmonic balance simulation of high-Q oscillators and highly nonlinear ring oscillators have been developed. The application of the frequency-domain harmonic balance method to relaxation oscillator simulation was also explored.

A globally convergent homotopy method is applied for robust high-Q oscillator simulation in the frequency domain. The method uses the idea of the voltage probe while requiring no initial guess for the probe voltage. Different embedding techniques have been evaluated and an efficient and robust algorithm has been demonstrated. A variety of high-Q oscillators as well as moderate-Q oscillators were simulated to show the validity of the new method. The developed algorithm can be easily applied to existing harmonic balance software by linking with the HOMPACT package.

Two novel ways of simulating ring oscillators with the harmonic balance method were also proposed. The phase relationships of a ring oscillator is exploited in both approaches. In the single-delay cell method, a single-delay cell equivalent circuit is developed for ring oscillator simulation. It is shown that the phase relationship can be easily and efficiently handled in the frequency domain. Details of the numerical formulation and implementation are given. With a reduced number of nodes and nonlinear devices involved in the simulation, the

single-delay cell method results in a significant improvement in the simulation time and convergence. This approach can also be applied to a flat netlist with the aid of subcircuit identification algorithms [46]. The proposed method assumes that all the oscillator cells are identical and cannot be used when large mismatches between cells need to be accounted for.

The proposed multiple-probe method can handle ring oscillator circuits with large mismatches in the delay cells. In the multiple-probe method, a voltage probe is applied to the input of the each delay cell. Although more than one probe is used, the new method requires no additional initial guesses compared with the conventional single-probe method. The use of multiple probes provides a method that is robust for ring oscillator simulation. Furthermore, this method is also efficient compared with the conventional method.

A variety of ring oscillator circuits have been simulated showing the validity of the two proposed approaches. If the delay cells in the ring oscillators are identical, the single-delay cell method is recommended for use, since it provides a significant speed up over the conventional method and the multiple-probe method.

The standard harmonic balance method is not suitable for simulation of the relaxation type oscillators due to accuracy problems arising from aliasing errors.

## **8.2 Future Work**

For some ring oscillators with complex delay cells, the frequency-domain harmonic balance simulation results in a large system matrix. Direct factorization of such a large matrix is time consuming and Krylov subspace methods should be used. However, since the ring oscillator is quite nonlinear, a conventional block diagonal preconditioner is not a good choice. More work needs to be done to find a suitable preconditioner.

In the single-delay cell method, the equivalent circuit used for simulation is based on identical delay cells. Extensions of this method to non-ideal delay cells needs further investigation. A sensitivity-like analysis can be used in conjunction with the single-delay cell method for small mismatches. The algorithmic approach needs to be developed and evaluated for both accuracy and performance.

It has been shown that the standard harmonic balance method is not suitable for simulation of relaxation oscillators. Some other approaches have been proposed to handle circuits with sharp transitions, such as the time-mapped harmonic balance method [47-48], the wavelet method [49-51] and multi-interval Chebyshev method [52]. However, it is not yet clear whether extensions of these methods to the simulation of relaxation oscillators is possible. The combination of frequency-domain and time-domain methods may also be a solution and needs further investigation.

**BIBLIOGRAPHY**

- [1] A. Hajimiri and T. H. Lee, *Design of Low Noise Oscillators*, Kluwer Academic Publishers, 1999.
- [2] K. S. Kundert, J. K. White, and A. Sangiovanni-Vincetelli, *Steady-State Methods for Simulating Analog and Microwave Circuits*, Kluwer Academic Publishers, 1990.
- [3] K. S. Kundert, "Introduction to RF simulation and its application," *IEEE J. Solid-State Circuits*, pp. 1298-1319, Sept. 1999.
- [4] K. Mayaram, D. C. Lee, S. Moinian, D. Rich, and J. Roychowdhury, "Computer-aided circuit analysis tools for RFIC simulation: algorithms, features, and limitations," *IEEE Trans. Circuits and Systems-I*, pp. 274-286, April 2000.
- [5] O. J. Nastov, "Spectral methods for circuit analysis," *Ph.D dissertation*, Massachusetts Institute of Technology, Feb. 1999.
- [6] D. Long, R. C. Melville, K. Ashby, and B. Horton, "Full-chip harmonic balance," *Proc. IEEE Custom Integrated Circuits Conference*, pp. 379 – 382, May 1997.
- [7] E. Ngoya, A. Suarez, R. Sommet, and R. Quere, "Steady state analysis of free or forced oscillators by harmonic balance and stability investigation of periodic and quasi-periodic regimes," *Int. J. Microwave and Millimeter-Wave Computer-Aided Engineering*, vol. 5, pp. 210-233, March 1995.
- [8] M. Gourary, S. Ulyanov, M. Zharov, S. Rusakov, K. K. Gullapalli, and B. J. Mulvaney, "Simulation of high-Q oscillators," *Proc. IEEE Int. Conf. Computer-Aided Design*, pp. 162-169, Nov. 1998.

- [9] M. Gourary, S. Ulyanov, M. Zharov, S. Rusakov, K. K. Gullapalli, and B. J. Mulvaney, "A robust and efficient oscillator analysis technique using harmonic balance," *Computer Methods in Applied Mechanics and Engineering*, vol. 181, pp. 451-466, Jan. 2000.
- [10] R. Neubert, P. Selting, and Q. Zhang, "Analysis of autonomous oscillators – a multistage approach," *Proc. MTNS Symposium*, pp. 1055-1058, July 1998.
- [11] L. T. Watson, S. C. Billups, and A. P. Morgan, "Algorithm 652: HOMPACT: a suit of codes for globally convergent homotopy algorithms," *ACM Trans. Mathematical Software*, vol. 13, no. 3, pp. 281-310, Sept. 1987.
- [12] L. Trajković, "Homotopy methods for computing dc-operating points," *Encyclopedia of Electrical and Electronics Engineering*, J. G. Webster, Ed., New York: John Wiley & Sons, vol. 9, pp. 171-176, 1999.
- [13] R. C. Melville, L. Trajković, S. C. Fang, and L. T. Watson, "Artificial parameter homotopy methods for DC operating point problems," *IEEE Trans. Computer-Aided Design*, vol. 12, pp. 861-977, June 1993.
- [14] J. Roychowdhury and R. C. Melville, "Homotopy techniques for obtaining a DC solution of large-scale MOS circuits," *Proc. Design Automation Conference*, pp. 286-291, June 1996.
- [15] D. Wolf and S. Sanders, "Multi-parameter homotopy methods for finding DC operating points of nonlinear circuits," *IEEE Trans. Circuits and Systems--1*, vol. 43, pp. 824-838, Oct. 1996.
- [16] W. Ma, L. Trajković, and K. Mayaram, "HomSSPICE: a homotopy-based circuit simulator for periodic steady-state analysis of oscillators," *Proc. Int. Symposium on Circuits and Systems*, pp. 645-648, June 2002.

- [17] W. Ma, "A simulator for periodic steady-state analysis of nonlinear circuits using homotopy methods," *M.S thesis*, Washington State Univeristy, May 2001.
- [18] H. G. Brachtendorf, S. Lampe, R. Laur, R. Melville, and P. Feldmann, "Steady state calculation of oscillators using continuation methods," *Proc. Design Automation and Test in Europe*, pp. 1139, March 2002.
- [19] X. Duan and K. Mayaram, "Frequency domain simulation of high-Q oscillators with homotopy methods," *Proc. IEEE Int. Conf. Computer-Aided Design*, pp. 683-686, Nov. 2004.
- [20] X. Duan, Y. Hu, and K. Mayaram, "Simulation of ring oscillators using the harmonic balance method," *Northeast Workshop on Circuits and Systems*, pp. 137-140, June 2004.
- [21] X. Duan and K. Mayaram, "A new approach for ring oscillator simulation using the harmonic balance method," *Proc. IEEE Asia South Pacific Design Automation Conf.*, pp. 236-239, Jan. 2005.
- [22] X. Duan and K. Mayaram, "An efficient and robust method for ring oscillator simulation using the harmonic balance method," *IEEE Trans. Computer-Aided Design*, Aug. 2005.
- [23] Y. Hu, X. Duan, and K. Mayaram, "A comparison of time-domain and harmonic balance steady-state analyses for coupled device and circuit simulation," *Northeast Workshop on Circuits and Systems*, pp. 93-96, June 2004.
- [24] Y. Hu, "Steady state analysis techniques for coupled device and circuit simulation," *Ph.D. dissertation*, Oregon State University, May 2005.

- [25] C. -R. Chang and M. B. Steer, "Frequency domain nonlinear microwave circuit simulation using the arithmetic operator," *IEEE Trans. Microwave Theory and Techniques*, vol. 38, pp. 1139 - 1143, Aug. 1990.
- [26] W. J. MaCalla, *Computer-Aided Circuit Simulation Techniques*, Kluwer Publishers, 1987.
- [27] P. Feldmann, B. Melville, and D. Long, "Efficient frequency domain analysis of large nonlinear analog circuits," *Proc. IEEE Custom Integrated Circuits Conference*, pp. 461-464, May 1996.
- [28] M. M. Gourary, S. G. Rusakov, S. L. Ulyanov, M. M. Zharov, K. K. Gullapalli, and B.J. Mulvaney, "Adaptive preconditioners for the simulation of extremely nonlinear circuit using harmonic balance," *Proc. IEEE MTT-S International*, pp. 770-782, June 1999 .
- [29] M. M. Gourary, S. G. Rusakov, S. L. Ulyanov, M. M. Zharov, K. K. Gullapalli, and B.J. Mulvaney, "The enhancing of efficiency of the harmonic balance analysis by adaptation of preconditioner to circuit nonlinearity," *Proc. IEEE Asia South Pacific Design Automation Conf.*, pp. 537-540, Jan. 2000.
- [30] R. Telichevesky, K. Kundert, L. Elfadel, and J. White, "Fast simulation algorithms for RF circuits," *Proc. IEEE Custom Integrated Circuits Conference*, pp. 437-444, May 1996.
- [31] F. Veerse, "Efficient iterative time preconditioners for harmonic balance RF circuit simulation," *Proc. IEEE Int. Conf. Computer-aided Design*, pp. 251-254, Nov. 2003.
- [32] S. K. Mitra, *Digital Signal Processing*, McGraw-Hill, 2001.

- [33] W. Anzill and P. Russer, "A general method to simulate noise in oscillators based on frequency domain techniques," *IEEE Trans. Microwave Theory and Techniques*, vol. 41, pp. 2256 - 2263, Dec. 1993.
- [34] A. Demir, A. Mehrotra, and J. Roychowdhury, "Phase noise in oscillators: A unifying theory and numerical methods for characterization," *IEEE Trans. Circuits and Systems- I*, vol. 47, pp. 655-674, May 2000.
- [35] D. Johns and K. Martin, *Analog Integrated Circuit Design*, John Wiley & Sons Inc., 1997.
- [36] D. O. Pederson and K. Mayaram, *Analog Integrated Circuits for Communication: Principles, Simulation and Design*, Kluwer Academic Publishers, 1991.
- [37] S. Lampe and R. Laur, "Global optimization applied to the oscillator problem," *Proc. Design Automation and Test in Europe*, pp. 322-326, March 2002.
- [38] E. L. Allgower and K. Georg, *Numerical Continuation Methods: An Introduction*, Springer-Verlag, NY, 1990.
- [39] R. J. Betancourt-Zamora and T. H. Lee, "Low phase noise CMOS ring oscillator VCOs for frequency synthesis," *2nd International Workshop on Design of Mixed-Mode Integrated Circuits*, pp. 37-40, July 1998.
- [40] A. Hajimiri, S. Limotyrakis, and T. H. Lee, "Jitter and phase noise in ring oscillators," *IEEE J. Solid-State Circuits*, vol. 34, pp. 790-804, June 1999.
- [41] P. N. Ashar, "Implementation of algorithms for the periodic-steady-state analysis of nonlinear circuits," *Memo. No. UCB/ERL M89/31*, Mar. 1989.

- [42] J. Maneatis and M. Horowitz, "Precise delay generation using coupled oscillators," *IEEE J. Solid-State Circuits*, vol. 28, pp. 1273-1282, Dec. 1993.
- [43] J. Lee and B. Kim, "A low-noise fast-lock phase-locked loop with adaptive bandwidth control," *IEEE J. Solid-State Circuits*, vol. 35, pp. 1137-1145, 2000.
- [44] R. Prasun, "A 0.6-1.2V low-power configurable PLL architecture for 6GHz-300MHz applications in a 90nm CMOS process," *Symposium on VLSI Circuits*, pp. 232-235, June 2004.
- [45] K. Mayaram, "CODECS: A mixed-level circuit and device simulator," *Memo. No. UCB/ERL MM88/71*, Nov. 1988.
- [46] L. Yang and C.-J. R. Shi, "FROSTY: a fast hierarchy extractor for industrial CMOS circuits," *Proc. IEEE Int. Conf. Computer-Aided Design*, pp. 741-746, Nov. 2003.
- [47] O. J. Nastov and J. K. White, "Grid selection strategies for time-mapped harmonic balance simulation of circuits with rapid transitions," *Proc. IEEE Custom Integrated Circuits conference*, pp. 13-16, May 1999.
- [48] O. J. Nastov and J. K. White, "Time-mapped harmonic balance," *Proc. Design Automation Conference*, pp. 641-646, June 1999.
- [49] N. Soveiko, "Wavelets for efficient algorithms in electronics design automation," *Ph.D. dissertation*, Carleton University, 2003.
- [50] D. Zhou and W. Cai, "A fast wavelet collocation method for high-speed circuit simulation," *IEEE Trans. Circuits and Systems-I*, vol. 46, pp. 920-930, Aug. 1999.

- [51] X. Zheng, S. Huang, Y. Su, and D. Zhou, "An efficient Sylvester equation solver for time domain circuit simulation by wavelet collocation method," *Proc. International Symposium on Circuits and Systems*, pp. 664-667, May 2003.
- [52] B. Yang and J. Phillips, "A multi-interval chebyshev collocation method for efficient high-accuracy RF circuit simulation," *Proc. Design Automation Conference*, pp. 173-183, June 2000.